TU Delft

Master Thesis by

Gale Dewo

Automatic Measurement of The Human Upper Limb Dimensions for Prosthetic Socket:

The Multiple Statistical Shape Model Approach

Automatic Measurement of The Human Upper Limb Dimensions for Prosthetic Socket: The Multiple Statistical Shape Model Approach

by

Gale Dewo

to obtain the degree of Master of Science
at the Delft University of Technology,
to be defended publicly on Tuesday October 30, 2018 at 10:00 AM.

ME51032
Student number: 4624254
Project duration: January 24, 2018 – October 30, 2018

Thesis Committee:

Dr. ir. Dick H. Plettenburg	3me TU Delft, chair
Dr. ir. Gerwin Smit	3me TU Delft, supervisor
Juan S. Cuellar Lopez, MSc	3me TU Delft, supervisor
Dr. Toon Huysmans	IDE TU Delft, supervisor

TU Delft Delft University of Technology

Acknowledgement

I have always been fascinated with the advancements of technology. Which is why I am very interested of this project when I heard it for the first time. However, during the process of conducting the thesis project, I realized that scientific research is not for everyone, including myself. Fortunately, I am blessed with generous supports from my family, friends, and supervisors.

Firstly, I would like to express my gratitude for Gerwin. From the first time I met you, I can already see that you are a critical person and also an open-minded researcher. I really enjoyed the discussions about the thesis, history, and religion with you. Congratulations to you and your wife for the twins. I would also like to thank Juan for having me in this interesting project. You have a noble purpose for your country and I am very proud to be a part of it. I hope you can succeed in achieving your goals. For Toon, thank you for all the help and discussion regarding this project. There were times when I felt unsure of my capability to formulate the algorithm for this project, but you helped me to get through it. For Bertus, thank you for helping me on the scanning experiment. I would like to thank Dick as the chair of the committee. Thank you for your insightful feedbacks. They are simple yet very critical for improving the project.

For the past two years, I have been studying in The Netherlands. Living in another country is a whole new experience for me. I am very grateful to have a new family and friends here. For Rafil, Putri, Ridho, Fajar, Adhi, Yusuf, and especially Etsa, you have always been there for me through thick and thin. I could not thank you more for everything.

Finally, I would like to say thank you to my family, Mom, Dad, Gaung, and my friends, Svida, Fathin, Aisyah, and Wisnu. You have always been supporting me even from Indonesia. Distance with you has taught me a valuable lesson about life and made me appreciate having you in my life more than ever.

Gale Dewo
Delft, October 2018

Abstract

An upper limb prosthesis, i.e. a hand prosthesis, is a device to replace the function of an upper limb on upper limb amputees. In developing countries, amputees' access to the device is scarce to unavailable. In addition to the absence of experts in those areas, currently there are no automatic measurement methods for upper limb amputees available. BME TU Delft Research Group is developing a solution for the issue by using a smartphone and 3D printing technology to provide access for the people in need.

The objective of this thesis is to automatically measure the dimensions from a digital 3D model of an upper limb stump which are required to create an upper limb prosthetic socket. The main method used in this thesis is Statistical Shape Modelling (SSM). We used Singular SSM and Multiple SSM as the approaches in this project. Geodesic distance and Intersection Line are used as measurement methods.

In order to validate the capability of the measurement algorithm to work with real human models, an experiment was conducted to test the precision of the algorithm. Nineteen participants with normal hands were 3D scanned. The manual measurement values were then compared with the values from the 3D scans by using both SSM approaches.

We propose an algorithm for automatic measurements of the human upper limb digital model for prosthetic application. The automatic measurement algorithm proved that we can measure real human upper limb for prosthetic application without human intervention. The Multiple SSM approach showed a sufficient result to be used in prosthetic application for upper limb socket. In the future, the resulting 3D-printed socket can be tested on upper limb amputees.

Table of Contents

List of Figures

List of Tables

Glossary

Objects/Terms:

- **Anthropometry:** Science about the measurement of the size, shape, and other features of the human body
- **Upper Limb Prosthesis**: Substitute or replacement of an upper limb on a human body
- **Artificial Cut**: Manual-made cut on the 3D model to imitate a residual arm
- **Antecubital Fossa:** Inside of the bend of the elbow region on the human upper limb
- **Olecranon:** Outer side of the bend of the elbow region on the human upper limb
- **Cut Length**: Residual arm length proportional to lower arm length (from elbow to wrist)
- **CAESAR**: Civilian American and European Surface Anthropometry Resource
- **Distal Belt**: Circumference near on the stump region area of the residual lower arm
- **Proximal Belt**: Circumference near on the elbow region area of the residual lower arm
- **Ulna Line**: Geodesic path from the wrist to the olecranon
- **Radius Line**: Geodesic path from the wrist to the antecubital fossa
- **Training Models**: 3D models which are used for building a statistical shape model.
- **Landmark**: Discrete anatomical loci that may be either biologically or mathematically homologous [1]; important point on the human body.
- **Principal Component/Shape Mode**: Limited set of values of linearly uncorrelated variables that shows the variance of the data
- **Geodesic Path**: The shortest path between two points on a curved surface
- **Intersection Line:** A line which is generated from the intersection of two surfaces
- **Regression Plane:** A 2D plane that minimizes the sum squared distance between points and the plane

Methods:

- **Uniform Remeshing:** Resampling of a surface to produce uniformly spaced vertices
- **Surface Registration:** A process to find correspondence between two surfaces
- **Screened Poisson Surface Reconstruction (SPSR):** A process to reconstruct a watertight surface from an oriented set of points samples.
- **Iterative Closest Point (ICP):** An algorithm to minimize the difference between two clouds of points over an iterative process.
- **Statistical Shape Modelling (SSM):** An analysis of geometrical properties from some given set of shapes (training shapes) by statistical methods. Consist of an average surface and shape modes
- **Principal Component Analysis (PCA):** Statistical procedure that reduces the variables of the data to convert a set of of variables into principal components which are ordered from the largest variance
- **Singular Value Decomposition (SVD):** A matrix factorization method for dimensionality reduction
- **Procrustes Analysis: A** method of statistical analysis which is used to compare the shapes of objects
- **Geodesic Measurement:** A measurement method by calculating the distance of a geodesic path

Chapter 1: Introduction

1.1 Background

An upper limb prosthesis, i.e. a hand prosthesis, is a device to replace the function of an upper limb on upper limb amputees. The function of the prosthetic device varies from cosmetic, daily use, and sports function. The device plays an important role to aid amputees perform physical activities which are limited by their disabilities.

For people in developing countries, access to hand prostheses are scarce to unavailable. There is no specialist that can easily be reached in these countries. The example of a real case is in Colombia. There are many upper limb amputees after Colombia civil war. According to the Central Military Hospital, the institution responsible for providing medical care to patients from the Armed Forces, anti-personnel mines used during the armed conflict in Colombia over the past 20 years have left 3,600 amputees from the security forces. About 10% of the amputees lost their upper limb [2]. However, the help from the government military is only about 64 prostheses distributed in 2017 [2]. At this rate, it could take more than 50 years only to help amputees from the security forces alone. The urgency to have a faster rate of distribution is hindered by the inadequate number of prosthetic experts in the area.

Taking advantage of mobile phone and 3D printing technology advancements, people at BME TU Delft have been developing an idea of 3D printed prosthetic devices that can be acquired by using a smartphone. We aim to provide access for the people in need of an upper limb prosthetic device. Since the usage of smartphones are common in developing countries, it is possible to scan or take picture of the amputee's remaining arm using the phone and send it to a computer to be processed. From these scan or pictures, we can obtain a user-specific upper limb prosthetic arm design to be manufactured with 3D printing devices, which are starting to become common everywhere and the cost to manufacture is relatively inexpensive. The cost of a 3D printed upper limb prosthesis is around $20 [3]. Whereas a cosmetic arm and hand might cost $3,000-$5,000. A functional prosthetic arm with a "split hook" at the end might cost $10,000. A myoelectric prosthetic arm with a realistic-looking, functioning hand might cost $20,000- $30,000 or more [4].

By introducing this solution, people who need a prosthetic device could get their own specific device without the need to find a prosthetic expert. Ideally, with this project everyone can obtain their prosthetic device with just a smartphone with internet connection. We wanted to create an upper limb prosthetic device from the 3D model of the patient upper limb stump without any human intervention. Providing a prosthetic device that can fit the patient means that we need to match the prosthetic socket dimensions with the patient's 3D upper limb stump model.

Therefore, this project is limited to the field of anthropometry, which is a science about the measurement of the size, shape, and other features of the human body [5]. There have been studies about the 3D anthropometry to measure a healthy human [5], [6]. However, studies on the 3D anthropometry for an amputee are very limited.

This thesis is part of the '3D printed hand prosthesis by using a smartphone' project. The contribution of this thesis is to provide an insight about how to automatically measure a 3D lower arm model, resulting in dimensions for creating an upper limb prosthetic socket as shown in Figure. Figure 1 shows how this thesis fits into the big project.

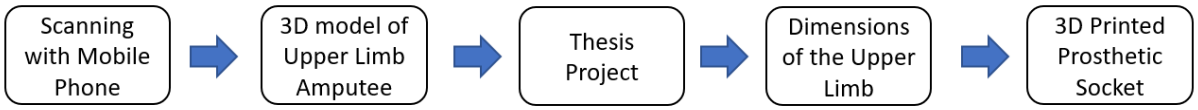

Figure 1. How the Thesis Project fit into the 3D printed prosthetic device acquired by smartphone.

Figure 2. Example of a Prosthetic socket

1.2 Problem statement

Conventionally, measurement of an upper limb to create a prosthetic socket needs an expert. However, in developing countries there are a limited number of experts to measure the patients. Therefore, an automatic measurement method of the upper limb stump is needed. Currently, there is no automatic measurement method for an upper limb amputee available.

1.3 Thesis Objectives

The objective of this thesis is to automatically measure dimensions from a digital 3D model of an upper limb stump which are required for creating an upper limb prosthetic socket.

1.4 Research question

We formulated a research question which arises from the measurement process of an upper limb amputee:

"How do we perform automatic 3D anthropometry in order to get upper limb dimensions for prosthetic application?"

This research question can be broken down into three sub-questions :

1. What are the measurements from the upper limb that are needed for generating a prosthetic socket?
2. What are the 3D anthropometry methods that are suitable to automatically measure the amputee upper limb?
3. How accurate is the automatic measurement by using this method?

These questions are the driving force of the project and should be answered throughout the thesis.

Chapter 2: Literature study

2.1 Automatic 3D Anthropometry

2.1.1 Overview

We conducted a literature study about Automatic 3D Anthropometry to know what has been done in this area and what we can do to improve and achieve the objective of the thesis.

Anthropometry, which is the science about the measurement of the size, shape, and other features of the human body [5], has been performed for years to document the statistical dimensions of human body parts. The results of the measurements have many uses in various fields such as medical, industrial design, automotive, fashion, military, virtual reality, etc. [5],[7]. Initially, experts performed anthropometric measurements with the traditional manual method such as using a ruler and measuring tape. The method is time-consuming and depended heavily on the operator's ability and consistency to measure different body parts [8].

Parallel with advances in photo imaging technology, 2D images are used in anthropometric measurements, and researchers have shown that the method is sufficient for industry use. Afterwards, since the last few decades, 3D image technology has been emerging and increasingly used in anthropometry, giving a more detailed measurement than 2D images.

At the beginning of 3D anthropometry, operators placed markers on the human body to identify important landmarks before the scan is performed. The accuracy and precision of the measurement depended heavily on the skill and consistency of the operator. This process is prone to human errors and time-consuming. There have been several studies to eliminate human intervention in the process. In order to facilitate the process, new methods have been developed to automatically measure distances between provided landmarks in the human model.

This literature study addresses the process between the input and the output of 3D anthropometry as shown in Figure 3, where the input is a human body model, and the output is a measurement result. This study also focuses on marker-less anthropometry, which is a method to locate landmarks and perform measurements without manually placing markers on the human body. By this approach, the need for time-consuming human intervention could be eliminated.

In the literature, this field of research is referred as the automatic method on 3D anthropometry. It is a highly researched field that shows promising results as well as eliminates time and effort required from landmarking the human body part.

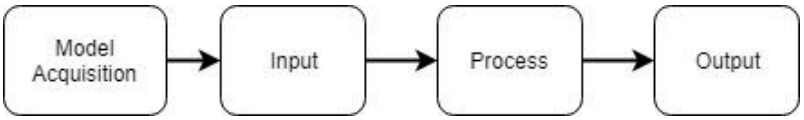

Figure 3. 3D Anthropometry Process. The Process starts with Model Acquisition of a Human Body. The Input will be either a 3D Mesh or Point clouds. It will be processed to produce The Output which will be used for other purposes.

We categorized automatic 3D anthropometry methods based on the research outcomes. Automatic

3D anthropometry workflow is divided into three processes: segmentation, landmarking, and measurement. Segmentation and landmarking are the primary steps before measurement. In the anthropometric measurement, segmentation could be initiated before landmarking or vice versa as seen in Figure 4. After that, the outcome of the process, which is a segment of body part or landmarks is measured based on what is required. The implementation of the processes that we have categorized vary between studies. There are a few papers which integrates all three processes such as Markiewicz et al., (2017) C. Lovato et al. (2009), Leong et al. (2007) and Lu & Wang (2008)[5], [9]–[11]. There is a small portion of the research that used manual landmarking and did the measurements in an automatic method such as Lee et al. (2010) [12]. The rest of the studies only do one or two categories out of three. Database of human anthropometry from projects such as CAESAR and FRGC are often used as a reference and material for research about 3D anthropometric measurement [6], [7], [13], [14].

Although the ultimate purpose of anthropometry is to measure dimensions of the human body, more research has been done on automatic landmarks extraction from an input model than research on measurement methods [15]. The reason is that landmark is really important in anthropometry measurement. Without landmarks, measurement cannot be done properly [16]. This statement is true because based on the standards[17]; measurements have to be based on landmarks. However, there is some research about measurements without the need of having a landmark. For instance, the work of Seoud et al. (2017) and Ding et al. (2010) where the purpose is to get measurements where the boundaries are unrelated to specific landmarks [18], [19]. This makes the accuracy of the measurement questionable.

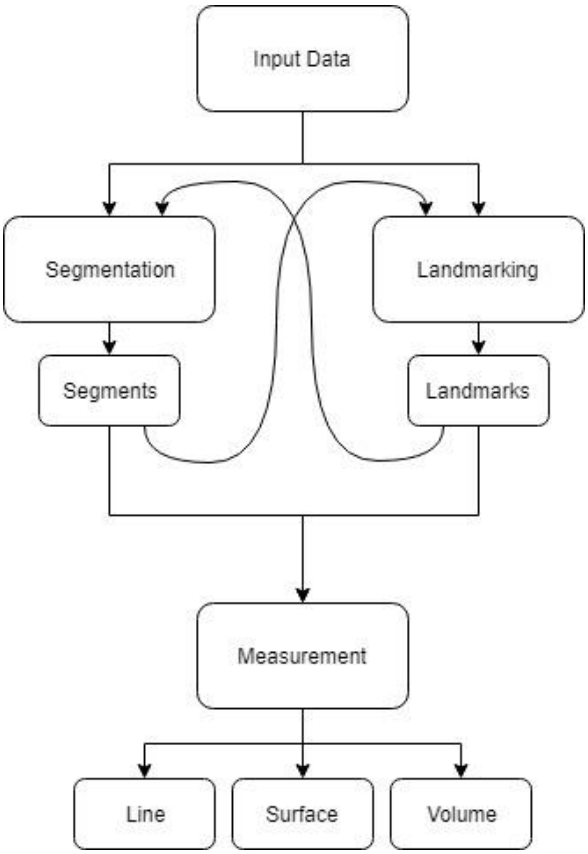

Figure 4. Flowchart of Automatic Anthropometry Measurement. The Input data can be processed with Segmentation or Landmarking to produce Segments and Landmarks, respectively. After both process, the final process is Measurement, to produce Line, Surface or Volume measurement values.

Anatomical landmark is defined as distinct regions or points on the surface with uniqueness in shape characteristics in their vicinity, and usually correspond to skeletal part features [7]. In the Geometric Morphometric Term, Landmark is a discrete anatomical loci that may be either biologically or mathematically homologous[1]. Bookstein (1991) originally defined three types of landmarks [20]:

- Type 1: discrete juxtapositions of tissues (i.e., the intersection of two sutures);
- Type 2: maxima of curvature (i.e., the deepest point in a depression, or the most projecting point on a process); and
- Type 3: extremal points or points that are defined by virtue of information at other locations on that object (i.e., the endpoint or centroid of a curve or feature).

This definition of Type 3 landmarks originally encompassed semi-landmarks, but Weber and Bookstein (2011) more recently redefined this system to identify Type 3 landmarks as those landmarks characterized by information from multiple curves and symmetry (i.e., intersection of two curves, or the intersection of a curve and a suture) and identified three subtypes [21].

These landmarks correspond to traditional anthropometric measurements, where an expert usually placed markers on the surface for measurement purposes. There are traditional standards of human body landmarking that are used as a reference for landmarks and measurement [22].

2.1.2 Segmentation

Segmentation of the body part is a separation of a specific body part from the rest of the body model. Segmentation of the input to a certain body part has some advantages. 3D anthropometry is a more complex method than its 2D counterpart, and as a result, computation power needed is much higher. Instead of dealing with a high number of points or meshes from the whole human body, it is desirable to have a certain part of the model which has the focus of the current anthropometric measurement. In some research, it is also better to have segmented body parts before searching for a specific landmark to avoid false positives and longer searching time [6], [23], [24].

In segmentation methods based on obtaining key landmarks; it is necessary to find the most salient points and landmarks which are easily visible. Based on those locations, it can be used for pose normalization of the model and division of the body parts before further use as shown by Fang(2011) and Guo et al. (2013) [25],[26]. Landmark-based segmentation has a simpler algorithm because the research does not need a different method for segmentation and landmarking as shown by Li and Zhong(2012) where the segmentation is a part of the landmarking process to achieve localized parts with intent to locate other landmarks that are harder to detect with higher accuracy [23].

Separating a specific body part such as breast for volume measurements could also be done by a landmark-based method as shown by Seoud et al.(2017) [18]. The negative curvature of the patient chest is defined as a delineation of the breast part, and the segmentation started on the base.

Various methods achieve segmentation of the body without having key landmarks. The simplest method is by using an anthropometric proportion to achieve a satisfactory segmentation result without using a complex mathematical model or high computation power. This method was applied in many studies such as Boukamcha et al. (2015) where the head-to-height proportion is known [13]. Also shown by Sghaier et al. (2016) where the proportion of forehead, eyes, and nose to the whole head is known from statistic anthropometry [27]. However, the result could be not quite accurate. Pose variation is also a problem for segmentation with anthropometric proportion because when measured in non-standard pose condition, there is a high chance that the segmentation can deviate outside the satisfactory range.

There are also segmentation methods based on a mathematical model of the surface. Giachetti et al.(2015) and Lovato et al.(2009) are using voxel coding method to extract a curve-skeleton from the target model [28], [29]. This resulted in lines and leaves (branches of the lines) that represent a generalized skeleton that can be further used to segment body parts. In the same research, the authors proposed to segment the body based on skeleton joints. However, it is not accurate enough without the help of landmark position. The method has an advantage that is insensitive to pose variation and therefore can extract curve skeletons from different non-standard poses.

Segmentation based on contour analysis for example is shown by Markiewicz et al.(2017) [5], their method is to slice the human body model from top to bottom. Based on the contour it can automatically detect which points are the neck, armpit and crotch locations in general. It determines where the model will be cut into segments of head, arm, torso, and leg. Another example in Leong et al. (2007), the segmentation is based on the grey level of the human body model, which represent depth [10]. The difference in grey values indicates extreme points where surface curves lies.

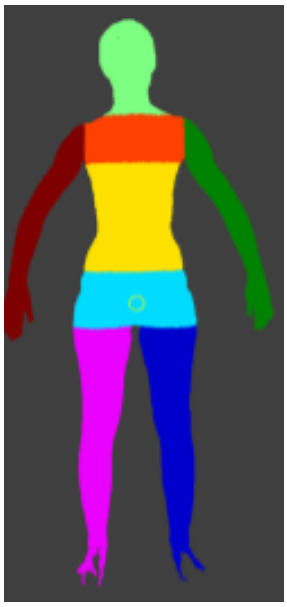

Figure 5. Segmentation of The Human Body by Markiewics et al.(2017). The algorithm separates each body part into individual segments.

In another work, segmentation of human body model in 3D can be simplified by having a 2D projection to a coronal plane, where the projection is represented as a silhouette and analysed for maximum local points to find the location of armpit and crotch. After that, the body is sliced in the horizontal plane where it meets the crotch point and vertical plane where it meets the armpit point [11].

The result of segmentation are segmented body parts which are used for further landmarking, and it yields a more accurate result and less time consuming than the whole body landmarking. Segments can also be used for further measurement of girth, surface area or volume, which is the ultimate purpose of 3D anthropometry.

2.1.3 Landmarking

Landmarking is the process of acquiring the location of a landmark from the human body. A great amount of research is done on how to extract landmark points without the need for human intervention. As stated by Markiewics et al. (2017), it can be concluded that the manual marking of landmarks by a human expert is time-consuming and the result is not consistent [5]. Processing a huge amount of different human anthropometry data will be bottlenecked by manual landmarking. Many researchers have clearly identified this problem, and this resulted in various methods to extract landmark location in a fully automatic way [15].

At first, research on landmarking is mostly done by putting markers in the human body before scanning. Some algorithm including color-based detection locate the marker position on human body scan. To some extent, this is quite a cumbersome approach. Because human intervention is needed for manual landmarking, it can take a long time to put all the markers precisely before scanning, resulting in declined accuracy when the operator is exhausted after working for a long time. Even after putting the markers there are still processing algorithm needed to capture the markers exact position. Example of this approach is shown by Lee et al.(2010) where they fabricated a plaster hand and marked it manually [12].

This approach is gradually replaced with an automatic marker-less method without human intervention, which is the focus of this literature review. By this approach, in the ideal condition, the only needed process with human intervention is to capture the human body into the 3D model, and the output would be the result of desired measurements. The process of manual landmarking is replaced by creating a relationship that describes landmark as a certain value. The computer can locate these landmarks in less time than the manual approach.

Landmarking process can be defined in two important steps as seen in Figure 6. In order to define a body landmark, it must be defined first what is the feature that describe the landmark. This feature can be described in a surface curvature value, texture, function, depth, etc. As stated by Liu et al.(2017), this is described as a local feature descriptor [30].

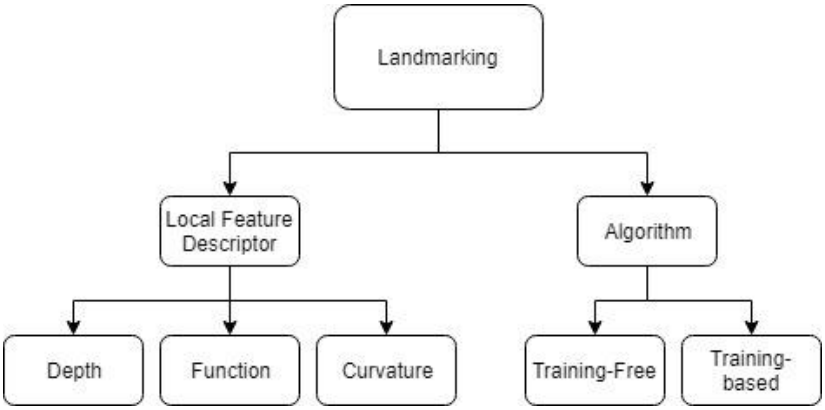

Figure 6. Landmarking Categorization. Landmarking has two important steps, Local Feature Descriptor and Landmarking Algorithm. Local Feature Descriptor describes important landmarks with a method based on Depth, Function, or Curvature principles. Landmarking Algorithm can be divided into training -free methods and training-based methods based on their need of a training data to build the algorithm.

After having a descriptor, landmarking process is run by an algorithm. These algorithms define how the local feature descriptors are defined and extracted. Landmarking algorithms are divided into training-based methods and training-free methods. Training-based methods are using samples or templates that have been pre-marked as a reference for the correct landmark locations. Landmarks of these templates are extracted to get the description of their local feature. Training-free methods are based on the prior knowledge of the landmarks. Some landmarks can be described with heuristic rules that is obvious and does not need a complex training process. For example, we can locate the tip of a nose by looking for the most forward point of the face. These methods can also be a linear process, which the next less apparent landmark is obtained from the previously detected landmarks which is more apparent [10], [26].

2.1.3.1 Local Feature Descriptor

An anatomical landmark can be described in an anthropometric way. Landmarks are derived from biological knowledge, specifically from anthropometry, the science of measuring the human body. Formally, ”A landmark is a point of correspondence on each object that matches between and within populations [31]”. However, obtaining a description to be used in a computational method is necessary for the program to detect it automatically.

A landmark can be described in multiple descriptions e.g. surface, spin images, grey level. There have

been many methods to describe landmarks based on the curvature, depth, texture, and function. The most common feature descriptor used in literature is the description of surface curvature, where the surface of a landmark can be described by using values of curvature. In the work of Markiewics et al.(2017), Boukamcha et al.(2017), and Suikerbuik et al.(2004), they use mean and Gaussian curvature to describe the surface which corresponds to the landmark [5], [6], [13]. Another author worked on maximum and minimum local curvature to define landmarks of the face [32]. A combination of curvature values with other methods was also demonstrated by Kermi and Laskri(2012) [33].

Sphere fitting is used to find a landmark such as a nose tip and an eyeball [26]. Laplace and Sobel mask is used to filter noise and detect feature before finding bending value of the surface [10]. Laplacian eigenvector and curvature is used to determine the surface properties [34]. Fang and Fang (2011) used the bending value of the surface to determine a landmark [25].

Kermi and Laskri (2012) stated that combining curvature values showed a better result than using them individually [33]. However, there was a contradictive finding where the combination of curvature values doesn't necessarily give the best result as stated by Abbas et al. (2015) [32]. Principle Component Analysis can also be used to get the local orientation of the surface normal [13].

Each landmark has its range of curvature value, and some landmarks could be represented by the extreme local value (change of direction in curvature). Curvature based feature is a fast, less time-consuming process. Another advantage of this approach is that the rotation of body will not affect its value. However, the accuracy is not accurate enough according to results, and it is prone to error [6].

Function-based feature descriptor is using a certain function that describes the landmark. The function ranges from the spin image, Fourier transformation, Hough transformation, heat kernel signature, etc. These approaches are more accurate than other approaches since it describes a landmark with precise detail. However, Fourier transformation is sensitive to changes of edges between the landmarks [7]. The approach is also considerably more time consuming, and for most of the method, it needs a pre-processing.

The spin image is a method that is actively used by the researchers as local feature descriptor. Johnson first proposed it in 1997 [35]. The spin image is a projection of 3D points into the 2D spin map. Each point in the model has a unique spin projection to it. In the work by Sukno et al.(2015) and Zhang et al. (2010), they are using the spin image as the local feature descriptor of target model to be matched to the template landmarks [35], [36].

Function-based descriptor can have a high computation cost, in the research by Liu et al [30]. the author is minimizing the spin image matrix into a vector by using Discrete Cosine Transformation. Another function-based descriptor is Discriminative Generalized Hough Transform. It is a descriptor that describes the appearance of an object from a reference point. It expands the method based on Generalized Hough Transformation by an iterative method and voting scheme [37].

Based on Laplace-Beltrami spectral decomposition, there are Heat kernel signature and Wave kernel signature as a feature descriptor. Heat kernel Signature is using auto diffusion function to describe the vector on a certain surface. Wave kernel Signature is using average probabilities of measuring quantum

mechanical particles with a defined set of energy levels in a certain point [38].

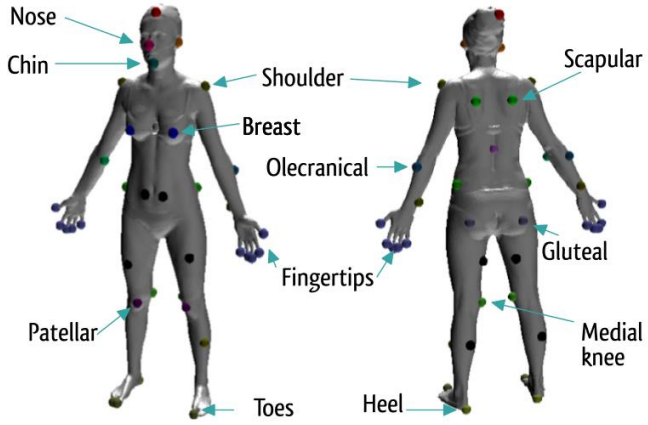

Figure 7. Automatic Extraction of Landmarks based on Wave kernel signature as shown by Lovato et al.(2014).

Feature descriptor based on depth is described by using depth image that represents the 3D model. This includes a grayscale analysis which corresponds to surface characteristics and used to describe landmarks [11], [25]. Loconsole et al. (2012) is using coarse spatial filtering which corresponds filtered 2D depth data with the 3D points [39]. Jahanbin et al.(2011) are using Gabor filter to process range images from an input of a combination of 2D and 3D images [40]. Gupta et al. (2010) are using colour and range images to determine landmarks for face recognition [14]. Guo et al.(2013) are using grey level as colour space to determine the sphere and convex fitting [26].

Texture-based feature descriptor requires the 3D model to be captured with the texture attached to the surface. This method is less common than other non-textured methods because it needs a higher degree of model acquisition. It is also prone to misalignment due to texture inaccuracy to the surface model. Naftel and Trenouth(2004) are using a texture based method by using visible light projections and surface texture [41].

2.1.3.2 Landmarking Algorithm

The procedure for obtaining local feature descriptor for extracting anthropometric landmark can be defined manually or by learning from another model. The algorithm of landmarking can be defined into two categories: training-based method and training-free method.

Training based method is an algorithm of landmarking that uses human body models with extracted landmarks as training samples. It will be used as a reference to find landmarks in other human body models. The samples features are extracted and learned to obtain data of each landmark description. The purpose is to get description without having a human to describe it manually. Since it is trained from different samples, the result would be accurate for most of the target sample. However, it would perform worse on samples with high deviation.

Training based method is a holistic approach to find landmarks. As stated by Gupta et al. (2010), 3D face recognition has more research in holistic approach than local approach [14]. Training based method examples are Hidden Markov Model, statistical shape model, template matching, active shape model, etc.

Hidden Markov model is a method that is based on learning relationship between certain models. Azouz et al. (2006) uses the spatial relationship between landmark as the basis of Markov model and probabilistic inference [42]. Another approach of Hidden Markov Model for training based method is also shown by Liu et al. (2017) [30].

Statistical shape model is a global approach that processes the template as a whole, not focused on each landmark [40]. Active shape model is a deformable template that matches target landmarks with the training set template [41], [43], [44].

Most training-based methods are using similarity function that calculates the similarity between target and template shape. Li and Zhong (2012) demonstrated the use of Euclidean distance as similarity function [23]. Combination of Euclidean and Geodesic distance is used by Jahanbin et al. (2011) and Gupta et al. (2010) [40], [14]. Hausdorff distance is used as similarity equation for template matching by Suikerbuik et al. (2004) [6]. Amberg (2007) and Li (2008) uses Iterative Closest Point to register between target and source [45], [46].

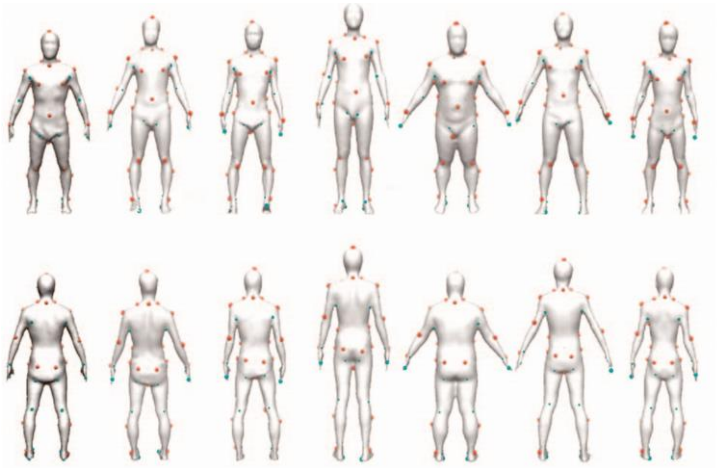

Figure 8. Template model (the first column on each row) that will be matching new targets(column 2 to 7) as shown by Li and Zhong(2012). Upper row are front view of the mdoels and lower row are back view of the models.

There is also candidate matching and template ranking, where there are multiple templates to be used. The template is matched to the target first by ranking based on the similarity. The candidate with the highest ranking will be used as the template for a certain target model [34].

Guo et al. (2013) set an algorithm for finding the most salient facial landmarks before applying a template to find the rest of the landmark. The result is then also included to be a reference face [26]. Liang et al. (2013) are using deformable transformation model to find more landmarks after the initial search [47]. Lovato et al. (2014) are using nearest neighbour classification to test the spectral descriptor and it outperforms other classifiers [38]. Discriminative iterative process is used by Boer et al.(2017) to expand the Generalized Hough transformation [48].

Training-free method differs from its training-based counterpart because this method does not need to be trained with existing samples before. The relation is built based on prior knowledge of the landmark such as position, distance, the value of feature descriptor, etc. Training-free method has an advantage for a smaller set of targets, since it does not need to be trained intensively for simpler

landmarks, and it does not need a lot of programming. A common approach is to have more salient landmarks to be extracted first before moving to other less visible landmarks.

Suikerbuik et al. (2004) set a heuristic range of values of curvature and function for every landmark, resulting in significantly less time needed for computation in comparison to template matching method [6]. Geometric relation between landmarks can be defined to search for other landmarks as shown by Sghaier et al. (2016) [27]. Han et al.(2010) shows a broad range of different torso shapes, they created a specific definition for each of the target landmarks. The landmarks are bust point, under-bust point, waist point, abdomen point, and hip point [49]. Specific definitions of the landmark from multiple descriptors and algorithms is presented by Leong et al. (2007) to obtain different landmarks using a step by step algorithm [10].

2.1.4 Measurement

The main process of anthropometry is to measure the distance between important human body landmarks. The measurement traditionally only consists of line measurement which calculates girth and length of certain distance. For medical purposes, there has been a consideration to measure certain surface area and body volumes of important body parts.

Standard for 3D anthropometry such as ISO 20685 has been established but researchers have not used it in their research. Markiewics et al.(2017) assessed their measurement with the standard . However, the result is not satisfactory. They stated that the standard is strict and quite unattainable [5]. Compared to traditional anthropometry, the automatic 3D measurement is significantly faster, but at the same time, it is prone to landmarking error [50].

Before automatic landmarking emerged, automatic measurement in the 3D model is based on manually marked landmarks. Li et al. (2012) are using cubic spline method to calculate the distance between the landmarks [51]. Wang et al.(2007) also shown automatic measurement with convex hull polygon method with a model of pre-marked human subjects [24].

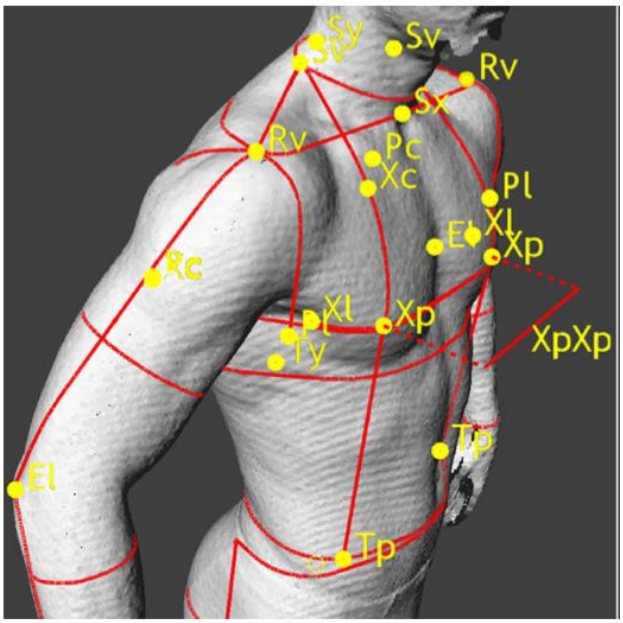

Figure 9. Template of Measurement Lines as shown by Markiewics(2017). After the landmark is acquired, the lines show the values of the target dimensions.

Lu and Wang (2008) were measuring linear and curvilinear distance by calculating the distance between landmarks and projecting the body into the sagittal plane and summing the line segments, respectively [11]. Markiewics et al.(2017) were calculating girth by using an algorithm to find the vertex of interest after the landmark is acquired [5]. Leong et al.(2007) have shown an algorithm for measurement to acquire lines for different body surface is obtained using 4^{th}-order B-Spline fitting and spatial plane intersection [10]. For area measurement, Lu and Wang(2008) were using convex hull polygon method to measure circumferences and cross-sectional areas [11]. Wassenmuller(2015) used a regression plane and preallocated lines on a template shape to get measurements from human body surfaces [52].

Volume measurement of a certain body part has correspondence with the health condition. Abnormalities could be an indication the symptom of a certain disease. For example, breast volume abnormalities could be indication for Adolescent Idiopathic Scoliosis [18]. Breast volume calculation is important to determine women health condition and potential of cancer. Seoud et al. (2017) measured the breast volume by separating breast from the trunk with a segmentation method. The volume is calculated with a ray tracing algorithm [18]. Body fat can also be estimated from the calculation various volume and surface area of trunk and other body parts as shown by Giachetti et al. (2015) [29].

Another advantage of automatic 3D anthropometry in measurement is that operator does not have to touch the subject directly in certain sensitive areas. In a traditional method with human as a measurer, it can cause discomfort for both operator and subject. As a result, the measurement is prone to error.

2.2 WILMER Open Socket

We present the overview from Pogosian (2015) about WILMER Open Socket which is the basis of the 3D printed socket design used in the project [53].

At Delft University of Technology, the WILMER Open Socket was developed for upper limb amputees within below elbow category, which is the amputation on the lower arm. The socket is designed based upon study of the forces transmitted between the prosthesis and the residual limb. It is an open socket that uses minimal area for fixation of the socket and leaves 75% of the skin uncovered [53]. This allows the skin to have more contact with air and in theory, perspiration problems that occurred in amputees with a closed socket can be minimized.

The socket consists of two rings enveloping the residual limb, distal ring and proximal ring. The distal ring is located near the tip of the stump and the proximal ring is located near the elbow. They are integrated with the forearm shaft. Together with the condyle brace that surround the upper arm, a complete socket is formed. The socket is constructed from stainless steel tubes and they are covered with soft foam to make it more comfortable to wear. Figure 10 shows how the two rings and the condyle brace fitted onto the residual limb [54]–[56].

The WILMER Open Socket allows easy use of the prosthesis by making the socket adjustable and ensuring a good fixation to the residual limb. With a locking mechanism the condyle brace can be locked into different positions. When pushing the button on the top of the prosthesis the locking mechanism can be released and adjusted into one of the 20 different positions with intervals of 1.3mm (Figure 11). The locking mechanism provides the prosthetic users an adjustable socket and a allowing for a more personalized fit. The amputees can tighten and loosen the socket anytime needed by themselves without the need of expert.

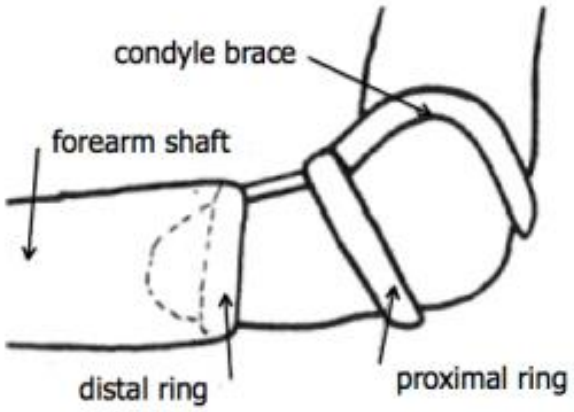

Figure 10. The distal - and proximal ring, and the condyle brace fitted onto the residual limb [55].

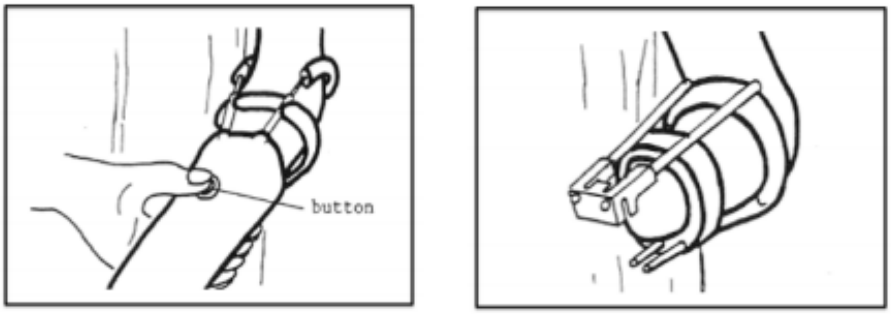

Figure 11. Left : Pushing button to release the locking mechanism. Right : The distal and proximal ring, and the locking mechanism fitted onto the limb [55].

The open socket is fitted directly onto the patient. This reduces the number of steps needed to produce a more correctly fitted read-to-wear socket [55]. Originally the WILMER socket was designed for children. The socket has been tested on several children in age between two and sixteen by Walta et al. (1989), and according to this study the open socket was highly appreciated by most of the children [55]. Other studies also showed that the adjustable socket is especially good for children since they constantly grow [54]–[56]. This can increase the longevity of the prosthesis.

The smart design of WILMER Open Socket provides an insight for the '3D printed hand prosthesis by using a smartphone' project. Moreo (2016) has successfully created a 3D printed prosthetic hand with parametric design for children [57]. However, the socket design is not there yet. The socket can be created by using 3D printer by tweaking the design to fit the additive manufacturing technique.

Chapter 3: Automatic Measurement Algorithm

3.1 Outline

In this chapter, we present a method to measure length and circumferences of a 3D upper limb stump model. Due to the nature of the upper limb amputation which has different length of amputations, we need to use a method which can handle variation while still providing an acceptable result. We decided to use statistical shape model as our main landmarking method, as it is a method which is more accurate than a training free method and it can be trained for variation of amputation cut lengths. We are using geodesic and intersection line as our measurement method.

As shown in Figure 12, first, we built statistical shape models from a database of 3D human model which have been refined with a reconstruction and remeshing method. After that we mark the important points and circumferences on the SSM mean surface. Finally, we match our Statistical shape models with the input 3D model to measure the required lengths and circumferences.

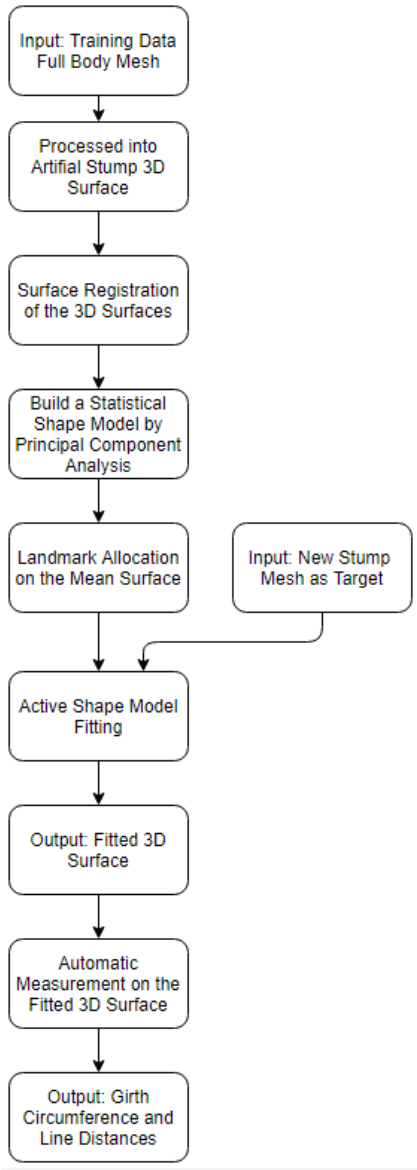

Figure 12. Automatic Measurement Algorithm

The main dimensions needed to create a socket are shown in Figure 13. We will assign the circumference line A-B as 'Proximal Belt', circumference line C-D as 'Distal Belt', line A-D as 'Radius Line', and line B-C as 'Ulna Line'.

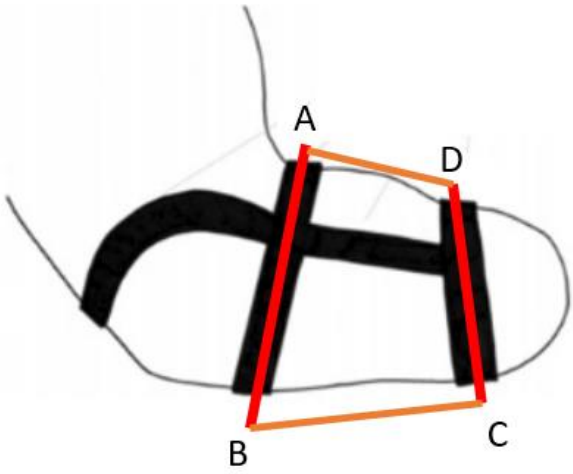

Figure 13. Dimensions needed to create a socket: Two Circumference showed by Red Lines (A-B and C-D), two lines showed by orange lines(B-C and A-D) connecting both circumference on the inner side and outer side of the lower arm.

3.2 Statistical Shape Model Building

3.2.1 Overview

Statistical shape model is a training-based algorithm for Automatic 3D Anthropometry. Basically, SSM is a surface that can morph into different shapes depending on its shape modes. The surface is an average of its training data, and the shape modes are the deformation vectors that built from the training data set. It is based on the active shape model with a statistical approach [44]. It is commonly used with objects that have variances such as human body because it can represent the variance very well. Due to the advancement of body scanning technologies, there are many models that can be used as the training data set to provide insights about the human body shapes.

We have decided to use Statistical Shape model as our landmarking method. This is due to the accuracy of the method compared to a training-free method. Our project of upper limb prostheses needed a good accuracy in measurement for the socket dimension and therefore, the SSM can provide this very well. The landmarks of the upper limb cannot be easily decided due to the abstract nature of the location and therefore SSM can predict where the landmarks are on the new target model. The reason why SSM can predict the landmark location is due to the prior knowledge of the different shapes of the arm and a previously established correspondence between these shapes. Knowledge of an important landmark can be captured in the system in the annotation of the Shape model. SSM also give a compact representation of allowable variation but are specific enough not to allow arbitrary variation depending on the quality of the registrations from the training data.

As presented by Cootes (2000), SSM is widely applicable [44]. The same algorithm can be applied to many different problems, merely by presenting different training examples. Therefore, we can use different training data for modelling a different case. A big variation of the residual arm after

amputation is observed. Therefore, we need to represent the different lengths of amputation in our Statistical shape model by providing training data set with different cut lengths.

To achieve different lengths of amputation from the model, we vary the lower arm cut with multiple variation based on the length proportion. We created four categories; wrist, 75%, 50%, and 25% cut. Different cuts are shown in Figure 14. With the multiple cut approach, we can simulate different length of amputation in the lower arm. The final results of the training data are 200 models of upper limb which is based from 50 base models with 4 different cut lengths for each base model.

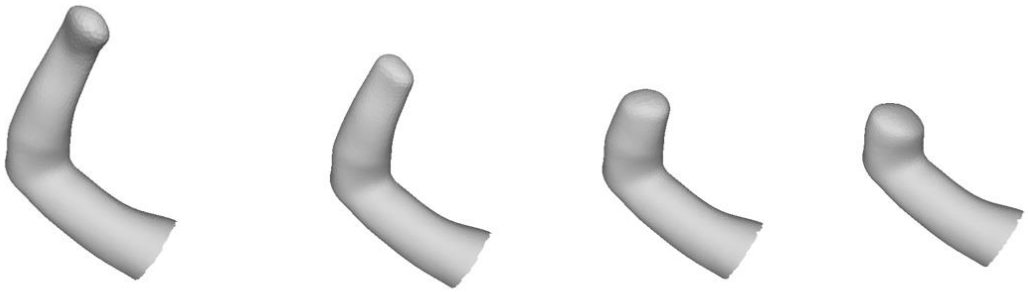

Figure 14. Different Cut Length of the Hand Stump. From Left to Right: Wrist Cut, 75% Cut, 50% Cut, 25% Cut

For our code, we created multiple SSM with different training sets. There will be two different approach for the SSM used in this research. For the first approach, we created an SSM that strictly contains models from a certain cut length. This means that we created an SSM exclusively for each category of cut. For example, the wrist cut 3D models are grouped as a wrist cut SSM, and this approach also applies to other cut lengths. For the second approach, we combined models with all cut length together. This means that we created an SSM with all models regardless of their cut length.

3.2.2 Approach

3.2.1.1 Singular SSM approach

The SSM training data for the first approach are all four categories of the cut from the wrist until the elbow. Having a wide range of cut length variation in the training data will result in more variance of the stump length. This SSM could represent all possible amputation lengths in the lower arm. This first approach is simple and does not need an added algorithm. In the later pages, we will call this approach as the 'General SSM'. The advantage of the first approach is that it can be used to fit all targets from different cut lengths. However, this approach also has potential drawbacks. The precision of the SSM could be compromised when it is fitting a target that is very different from the mean surface. When the SSM is morphing into a much larger target, it could give underestimation of the target and the vertices could have undersampling, giving a less detailed surface. It could also pose a problem when the SSM is morphing into a much smaller target. The resulting surface could be very dense with vertices but could not give a correct representation of the target surface because of limited target points that can be corresponded with.

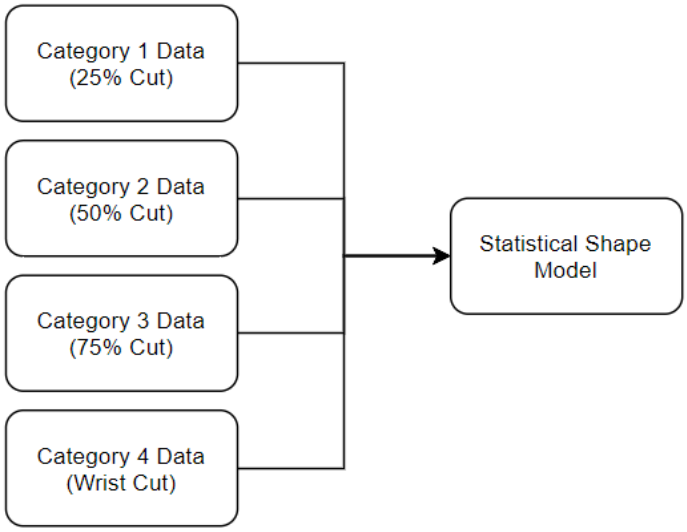

Figure 15. General Statistical Shape Model

3.2.1.2 Multiple SSM approach

The second approach is to have different SSM for each cut category. The hypothesis is that with specialized SSM, the precision of the Shape model will be better towards a specific cut length. We decided to have four categories; wrist, 75% 50%, and 25% cut. Zhou and Hao(2017) have shown that this approach could provide a better starting template for landmark annotation of a target shape [34]. We adopted this approach in our Multiple SSM approach to take advantage of a different SSM in fitting a different cut length target. We could predict in which category does one model belong to by knowing which SSM deformed the least when fitting into the target. In the later pages, we will call this approach as the 'Specialized SSM'. This approach has an advantage of better precision because each SSM is specialized for certain target. However, in some cases there may be a misfit because of wrong ranking algorithm. Especially when a target is an outlier or is posed similar to the other category where it should not be.

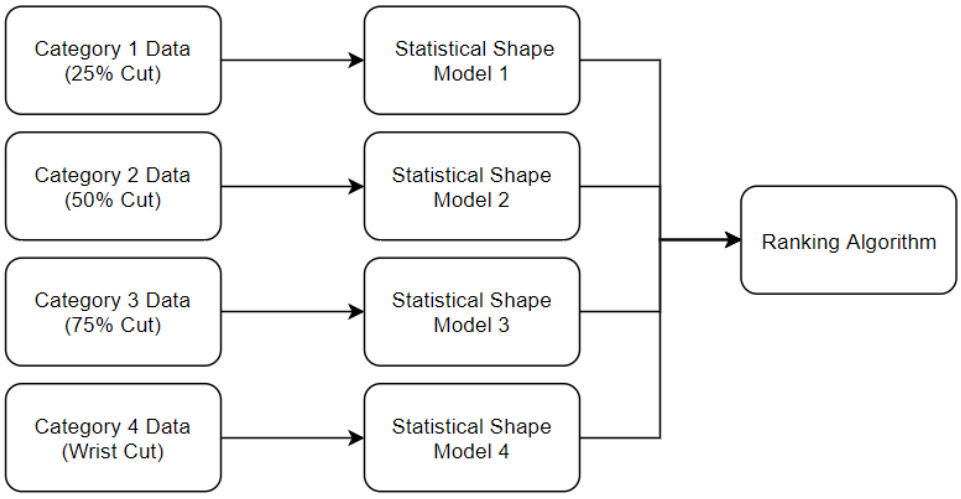

Figure 16. Specialized Statistical Shape Model

3.2.3 The Preparation of The Training Data

3.2.3.1 CAESAR 3D Model

In this section, the objective is to prepare training data for the statistical shape model.

In order to build a SSM, it is required to have multiple training data models of amputated upper limbs. However, it is very difficult to get real upper limb stump models from clinics due to confidentiality issues. We have come up with a solution to use a full body model from CAESAR database. We have 50 human body models from CAESAR database. One example of the model is shown in Figure 17. However, the model surfaces are incomplete (have holes). The pose on the models are not perfectly adjusted. There are variances on the pose especially the arm posture. This makes it difficult to automate segmentation of the hand from the rest of the body model. Therefore, the segmentation of the hand was done manually. We cut the model from the shoulder area, and then also cut it in the lower arm. The result from this step are 50 models of segmented upper limb as shown in Figure 18.

Figure 17. Example of a CAESAR 3D model

3.2.3.2 Screened Poisson Surface Reconstruction

In this step, the objective is to reconstruct a normal upper limb into a surface which looked like a amputation stump. Furthermore, we wanted to have variation of the amputation length in four different categories.

The upper limb is reconstructed with the Screened Poisson Surface Reconstruction from Kazhdan(2013) method as shown in Figure 18. Poisson surface reconstruction creates watertight surfaces from oriented point sets. the screening term is defined over a sparse set of points rather than over the full domain [58]. This method gives a smooth and natural surface. The validity of the reconstruction is approved by an expert in prosthetics. The reconstructed artificial cut of the upper limb is shaped similar to a clean amputation type. This process is done in Meshlab software.

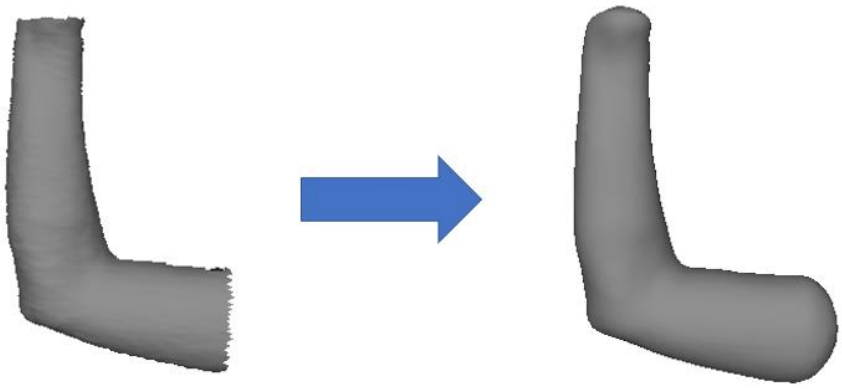

Figure 18. Screened Poisson Surface Reconstruction. Left: Segmented Upper limb Surface, Right: Surface reconstructed with Screened Poisson Method to mimic amputation stump.

3.2.3.3 Uniform Remeshing

In this step, the objective is to have the mesh uniformly spaced.

The number of vertices has effect on processing time and accuracy of the model. The model with lower number of vertices will give faster processing time because the model only needs a low computing power. However, since the number of the vertices is lower, details of the model can also be lost if the original mesh is converted into a lower resolution mesh. Later, we will do a surface registration by using a vertex-to-vertex Iterative Closest Point, this method requires uniform spaced vertices on the training models to avoid false point matching. We achieve this by remeshing the models uniformly with ACVD, a software specialized for surface coarsening and resampling. The clustering of the surface is driven by the minimization of a discrete energy term. The minimization approach is enhanced by generalizing the notion of Voronoi Diagrams [59]. The model vertices number can be determined by the user and the result is a uniformly spaced mesh.

The models are uniformly meshed with the ACVD software. We tried several values for the number of vertices in order to have a balance between detail and computation cost. In the end, the optimal vertices number is 3750. Which gives a detail near to the input quality mesh while giving a low computation time of surface registration. The result of the mesh from this process is shown in Figure 19. This resulted in 50 x 4 stump models with uniformly spaced mesh, where all of these models will be the training data set for the SSM.

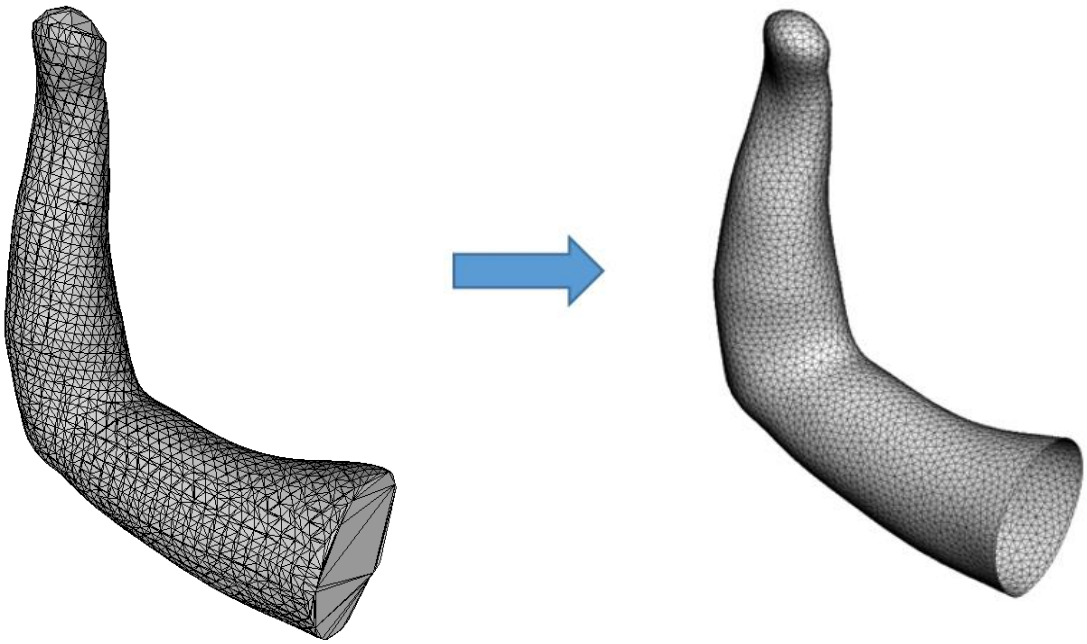

Figure 19. Uniform Remeshing Process. Left: The Artificial Cut Surface, Right: Uniformly Remeshed Surface

3.2.4 Surface Registration

3.2.4.1 Overview

In this section, the objective is to process all training data to have the same number of vertices and the vertices ID in a similar position. This can be achieved by establishing correspondences between all surfaces in the training data. Figure 20 showed what will be done to the training data in this section.

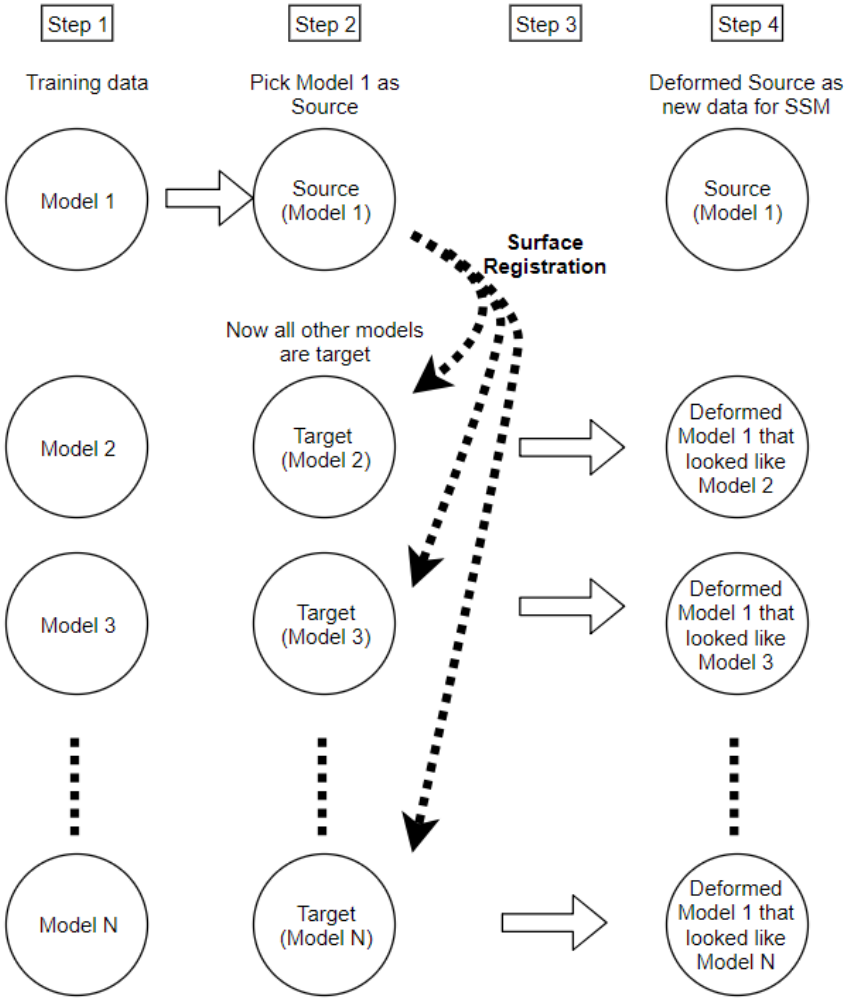

Figure 20. Four steps in Building a proper data for the SSM. In step 1, the models have different number of vertices and vertex ID. In step 2, we choose Model 1 as a source, and all other models become the target. In step 3, we do surface registration process from the source (Model 1) to all other targets. In step 4, the end results of Deformed Sources shaped like all targets and now they have the same number of vertices because it is based from Model 1.

Registering two surfaces means finding a mapping between a source surface and a target surface that describes the position of corresponding points [45]. A point of source surface is required to be in correspondence with a certain point in the target. This also applies to every single point in the model as shown in Figure 21.

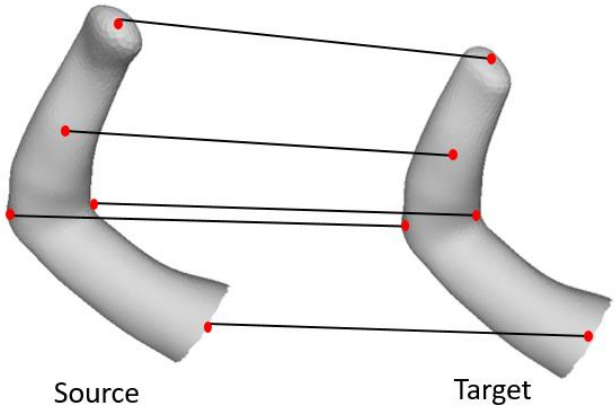

Figure 21. Surface Registration. Matching Points from Source (Left) to Target (Right)

When building a SSM, the number of the points are required to be the same between all training data. Therefore, after the surface registration process, the training data are in correspondence and after that, mean shape and shape variance could be calculated. We present the process of the surface registration which incorporated Rigid and Non-Rigid ICP is shown in Figure 22.

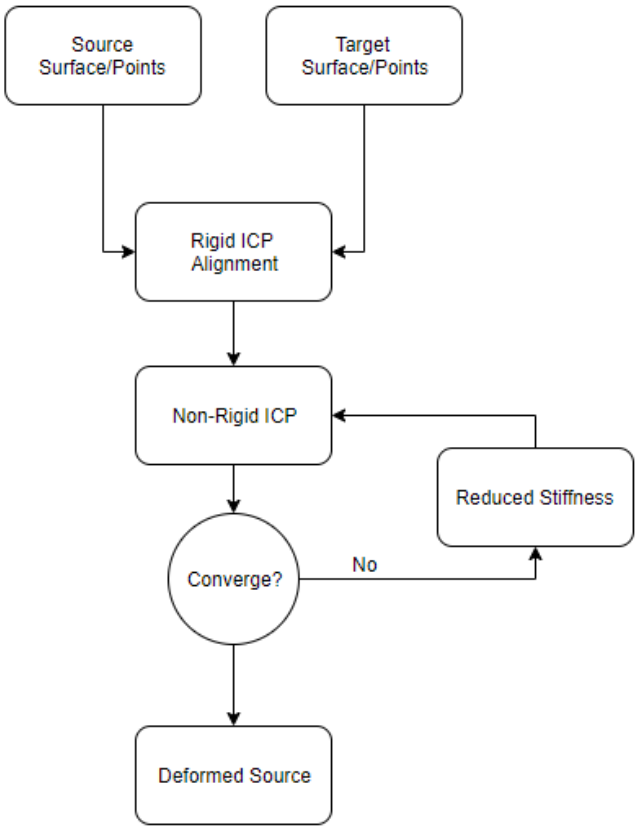

Figure 22. Flowchart of Source Surface Registration to Target Surface by Using Rigid Transformation and Non-Rigid ICP

Surface registration is a process to find correspondence between two surfaces. It will determine which point in the source surface that is represented in the target surface. We register the surface by rigidly

transforming and locally deforming the source into a target surface. The result of this process is a deformed source surface which shaped like the target surface as shown in Figure 24. By applying this process to all training models, all training models are now represented with new surfaces which have the same number of vertices and connectivity (triangles). Finding the corresponding point between two surfaces is essential for building a Statistical Shape Model, since the number of variables from different subjects is required to be the same. The quality of the found correspondence is very important, since it will determine the quality of the SSM surface and shape modes.

We build the SSM in MATLAB environment. First, we need to convert the 3D model into data of faces and vertices. The vertices are represented in 3D Cartesian point coordinates (x,y,z). The faces represent a triangular mesh which where each face is built from three vertices and where faces sharing two vertices are connected to each other. The duplicate vertices that does not belong to a face are then removed. At the end, the number of faces (F), egdes (E) and vertices (V) of the surface are in accordance with Euler's polyhedron formula $V - E + F = 2$ [60]. We also compute normal vector of each faces.

At the first iteration, we chose one random model to be the reference. This reference or source surface will deform into 39 other targets in the surface registration process. At first, we cannot decide which model is the best reference, but it can be solved after the registration by using the average surface of all the training models as the reference. Therefore, we have done more than one iteration of the surface registration to remove the bias and achieve a good result.

Before the surface registration process, we align every training data with the source surface by using Procrustes analysis without scaling component [61]. The Procrustes analysis will be used on later for rigid transformation. Another feature that can be done to improve the initial alignment is to have important landmark points marked before the registration. These landmarks can be aligned on the instead of doing Procrustes analysis of all vertices. However, in some cases this proven to be a difficult and intensive task. It also negates the time advantage of the automatic process. Therefore, we do not use landmark processing in this step.

The pseudocode for the surface registration process is as follows:

1. Initialise the alignment between source and all target using Procrustes analysis without scaling.
2. Moving to the surface registration loop for each specific target
    a. Update the corresponding point using a closest point method and normal value.
    b. Determine the weight of source vertices by using normal value dot product for each corresponding pair.
    c. Perform rigid transformation.
    d. Perform non-rigid deformation by using non-rigid ICP based on Li, minimize the total energy function.
3. Check for convergence, if not converged repeat step 2 with reduced stiffness so the vertices can move further.
4. Establish final correspondence by finalizing the latest deformed source.

3.2.4.2 Rigid Transformation

The objective of this step is to align a source surface with the target surface.

The surface registration is done by iteratively transforming source surface into the targets shown in Figure 23. First, rigid transformation is applied to minimize the distance between the two surfaces. At this stage, the final correspondence is not yet known. It is done by an iterative closest point method. The reference undergoes rotation, translation, and scaling to match the target. It is done until the sum of average error (root mean square) between source and target achieved the minimal value [61]. At this stage, the final correspondence has not established yet. Therefore, our calculation is using a closest point correspondence which changes through iterations. Normal vectors are involved in determining the confidence weight for a corresponding points pair. Good agreement of the normal at the source and the normal at the target point results in high confidence weight.

The source vertices are deformed by the rigid transformation so that a vertex x_j is transformed to $\tilde{x}_j$according to

$$\tilde{x}_j = \Phi_{Rigid}(x_j)$$

The global rigid transformation defined by a scaling factor **s** rotation matrix **R** and a translation vector **t**. The rotation is relative to the center of mass of the target.

$$\Phi_{Rigid}(x_j) = sx_jR + t$$

The rigid transformation is a very important step in the surface registration. Usually, a rigid transformation undergoes a translation or rotation to align the two objects together, A proper result from rigid transformation means that the process recognize two objects similarities and correspondence can be achieved with a closer distance after. The process resulted in a sufficient transformed surface for further deformation process. The Rigid transformation process is illustrated in Figure 23.

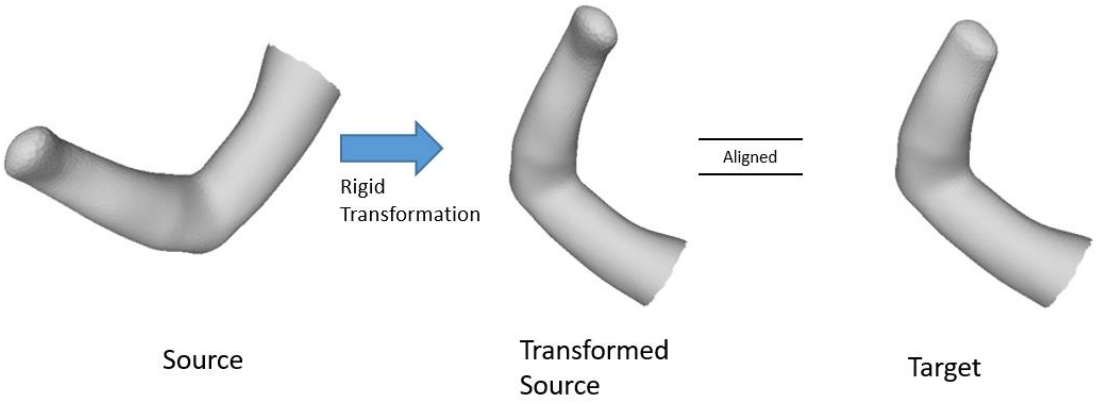

Figure 23. Rigid Transformation. Left: Source Surface, Centre: Result Surface from Rigid Transformation to match Target, Right: Target Surface.

3.2.4.3 Non-Rigid Iterative Closest Point

The objective of this step is to make the aligned source surface become shaped like the target.

After the rigid transformation, a non-rigid transformation is applied by translating the vertices locally to match the target. Initially, we used two method non-rigid ICP which is based on Amberg (2007), and Li (2008) [45], [46]. However, we found out that the method based on Li is more robust when dealing with missing vertices. Therefore, we continued the non-rigid ICP with the local optimisation method based on Li. The Non-rigid ICP is a method to locally deform points from the source(reference) to the target. The illustration is shown in Figure 24.

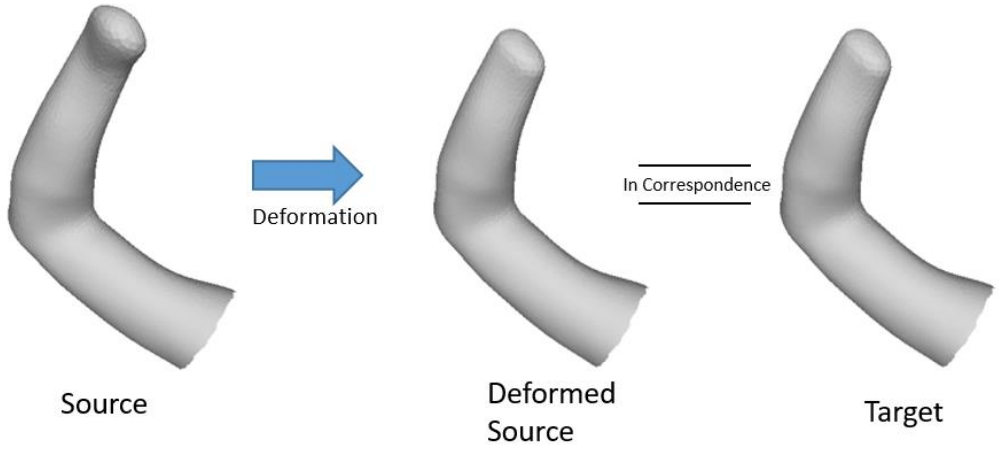

Figure 24.Non-rigid deformation. Left: Source Surface, Centre: Result Surface from Non-Rigid ICP to match Target, Right: Target Surface

The source will find the closest points in the target surface with similar normal values and it is done iteratively after the deformation. By matching each point to a corresponding point, the overall error is known. However, when a source point is corresponding with a target that has distance significantly higher than other corresponding distances, the confidence weight is lower than those corresponding distance with lower distances. When the confidence weight is reaching zero, a certain point will only

move along with its neighbour without looking for a match. This will be useful to avoid an abnormal shape of the final correspondence and to cover holes that could be present on the target. The Rigidity term controls the movement of neighbouring vertices. The illustration of the Non-Rigid ICP is shown in Figure 25.

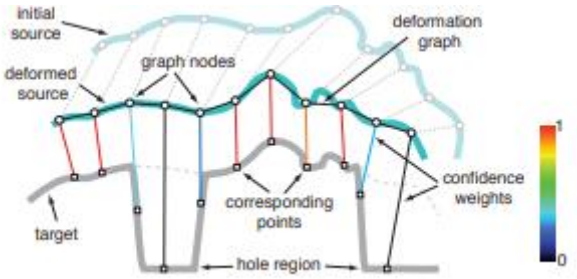

Figure 25. Non-Rigid ICP Process Illustration. Initial Source (Top) is morphing to the Target (Bottom). Result is Deformed Source(Middle). Source: Li(2008)[46]

The non-rigid ICP from Li (2008) principle is to minimize the total energy function from different terms.

$$E = \alpha_{Rigid}E_{Rigid} + \alpha_{Smooth}E_{Smooth} + \alpha_{Fit}E_{Fit} + \alpha_{Conf}E_{Conf}$$

The first energy term, E_{Rigid} ,penalizes the deviation of each transformation from a pure rigid motion. Consequently, local features deform as rigidly as possible avoiding shearing or stretching artifacts. The second energy term, E_{Smooth} , serves as a regularizer for the deformation by indicating that the affine transformations of adjacent graph nodes should agree with one another. The third energy term, E_{Fit} , which strives to move each source graph node to its corresponding position on the target shape. This allows the corresponding points to move along the surface of the target. This parameter is a key ingredient of Li's method. It automatically constrains the corresponding points to lie on the target scan and avoids the need for re-projection during the optimization as in the case of non-rigid ICP approaches. The last energy term, E_{Conf} , is the confidence energy term which maximizes the region of overlap to achieve higher confidence level [46]. For further explanation of the Non-Rigid ICP, readers could refer to Li (2008) [46].

The adaptation of weights α initially favors global rigid transformation and subsequently lowers the stiffness of the object to allow increasing local deformation as the optimization progresses [46]. The non–rigid transformation is continuously done until all points reached its convergence.

Figure 26. Overlapping Surface, Result of the Non-Rigid ICP. Yellow surface is the Deformed Source. Purple Surface is the Target Surface

The surface registration process is done to all targets, resulting in fifty 'deformed source models' which are shaped like all the training data including the reference for each cut category. Every model in each category now has the same number of faces and vertices.

3.2.5 Principal Components Analysis

The objective of this section is to create a Statistical Shape Model, which consist of a mean surface and shape modes or principal components.

The Statistical Shape Model is built from the 40 deformed surfaces that resulted from the surface registration. We excluded 10 deformed sources that has significant error or failed when registering the surfaces. The SSM is based on the Principal Component Analysis of the data. We want to find the directions in the data with the most variation, i.e. the eigenvectors corresponding to the largest eigenvalues of the covariance matrix, and project the data onto these directions.

Principal Component Analysis (PCA) allows us to find the major axes of a cloud of points in a high dimensional space. This is useful, as we can then approximate the position of any of the points using a small number of parameters. Given a set of vectors {xi}, we apply PCA as follows.

1. Compute the mean of the data.

   The mean surface is obtained by averaging all point coordinates. First, all of the deformed models are rigidly transformed with the Procrustes analysis in order to align them correctly as shown in Figure 27. After that, we put all vertices coordinates in a single matrix and calculate the mean value for each vertex.

$$\bar{x} = \frac{1}{n}\sum_{i=1}^{n} x_i$$

The mean value for each point is then rearranged as the mean surface. The mean surface of the general SSM is shown in Figure 28.

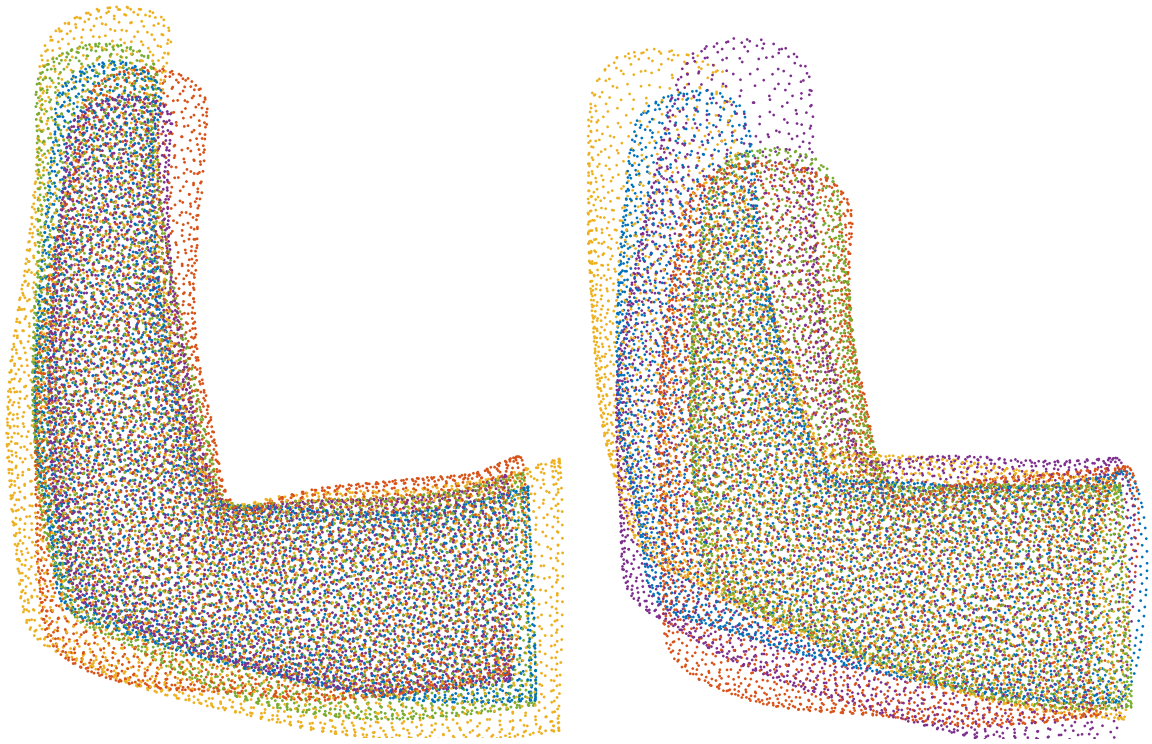

Figure 27. Procrustes Analysis. Points of deformed surfaces from training data set are aligned together. Left: Points from 75% cut models sample. Right: Points from All of the models sample.

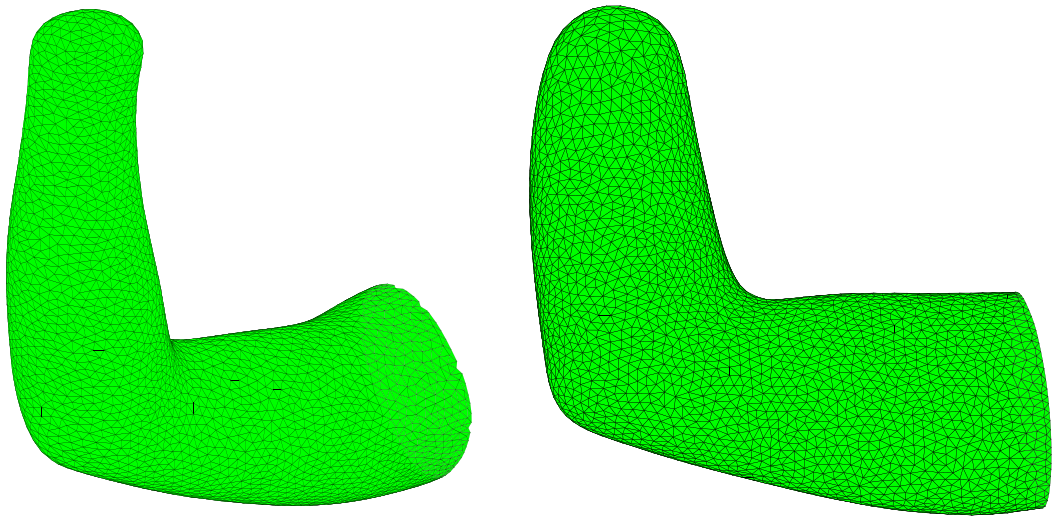

Figure 28. Mean Surface from the deformed surfaces. Left: Specialized SSM of 75% cut. Right: General SSM

2. Compute the covariance of the data,

Using a Singular Value Decomposition(SVD), we can compute the covariance of the data. First, we decompose X by using SVD

$$X = U\mathbb{\Gamma}W^T$$

And then we can write the covariance matrix as

$$C = \frac{1}{n}XX^T = \frac{1}{n}U\mathbb{\Gamma}^2U^T$$

3. Compute the eigenvectors, p_i, and corresponding eigenvalues, λ_i , of C
4. Each eigenvalue gives the variance of the data about the mean in the direction of the corresponding eigenvector. Compute the total variance from $V_T = \sum_t \lambda_i$
5. Choose the first t largest eigenvalues such that

$$\sum_{i=1}^{t} \lambda_i \geq f_v V_T$$

where f_v defines the proportion of the total variation one wishes to explain (for instance, 0.98 for 98%)

After building the SSM, we can define a surface X by tuning the weight(***b***) of the principal components(P). It is formulated by equation

$$X = \bar{x} + Pb$$

The Principal components are sorted based on the overall variance that it contributed. The biggest variance is defined as the first principal component, where the next biggest variance is the second principal component and so on. It is shown in Figure 29 the variances from principal components of the general SSM.

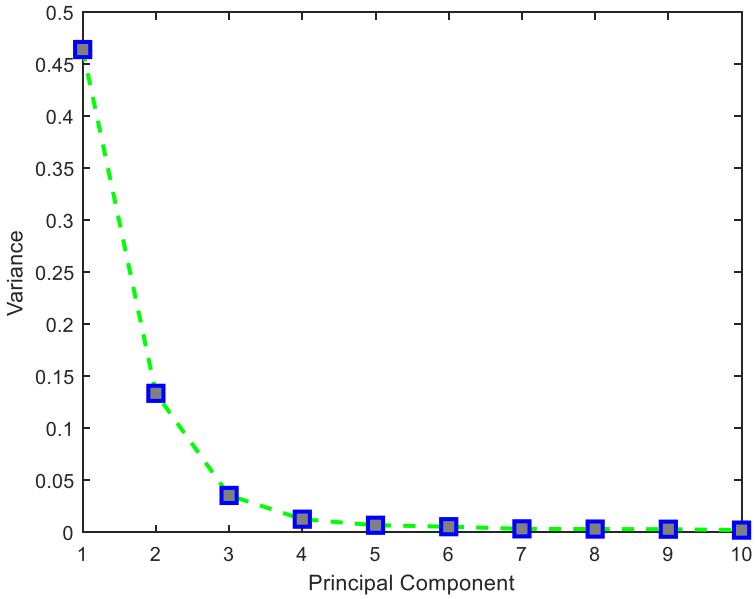

Figure 29. Scree plot of The General SSM principal components. Vertical axis is the variance, Horizontal axis is the Principal Component Number

To Illustrate the first principal component (shape mode) that holds the biggest variance, we could see the representation of the first principal component in +3 and -3 of its Standard Deviation value. In this example we are turning the values of the first PC of the general SSM into the edge of the distribution. The morphing in the first principal component of the General SSM is shown in Figure 30. The morphing in Specialized SSM first principal component of different cut length categories are shown in Figure 31.

Figure 30. Resulting surfaces in direction of the first principal component (shape mode) of the General SSM. Left: -3 Standard Deviation, Centre: Mean Surface, Right: +3 Standard Deviation

Figure 31. Resulting surfaces in direction of the first principal component (shape mode) of the Specialized SSM in 25% length cut. Left: +3 Standard Deviation, Centre: Mean Surface, Right: -3 Standard Deviation

Figure 32. Resulting surfaces in direction of the first principal component (shape mode) of the Specialized SSM in 50% length cut. Left: +3 Standard Deviation, Centre: Mean Surface, Right: -3 Standard Deviation

Figure 33. Resulting surfaces in direction of the first principal component (shape mode) of the Specialized SSM in 75% length cut. Left: +3 Standard Deviation, Centre: Mean Surface, Right: -3 Standard Deviation

The figures show that the first principal component of the General SSM seems to represent the different cut length, where it is very logical that the different cut length will have the biggest variance. The Specialized SSM different categories also showed variance of arm sizes. The difference in lower arm length is not dominant because each category only resembles models within specific cut length. And therefore, we can say that the SSM is working perfectly by showing the biggest variance of the training data set.

3.2.6 Landmark Annotation

The objective of this section is to mark 'important landmark' points on the mean surface of the SSM.

The SSM average surface consist that can be morphing into new target. Before the fitting, we manually marked important landmark points on the average surface as shown in Figure 34. We marked the wrist bones, the tip of the stump, the olecranon, and the antecubital fossa. We also marked multiple points as a belt around the Distal Belt and the Proximal Belt as shown in Figure 35. These points will be used later after fitting into a new target to find the distances and circumferences.

This is a simpler approach than to have manually marked the training data set from beginning one by one because that would be a labour-intensive task. We tried several annotation sets and see the fit result later to decide which one is the most suitable annotation.

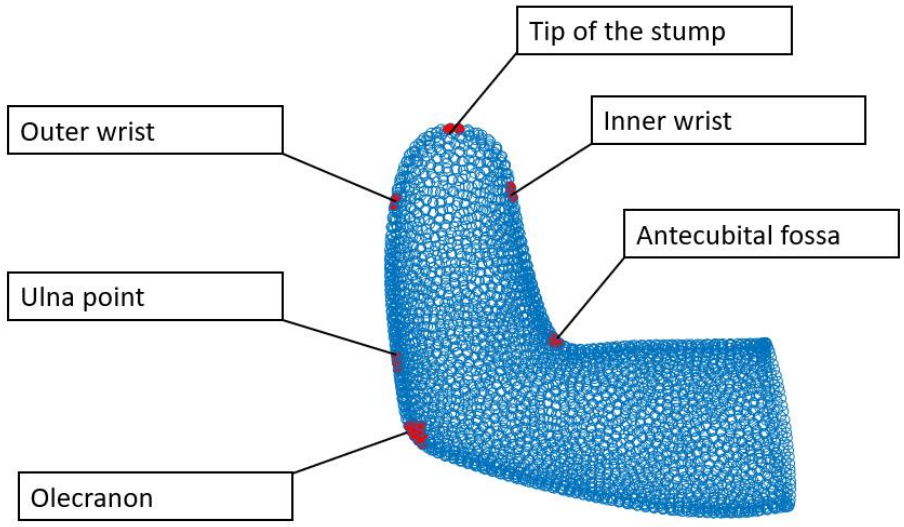

Figure 34. Landmarking the Points From the Mean Surface. The Red Points Indicate wrist, olecranon, ulna point, antecubital fossa, and tip of the stump

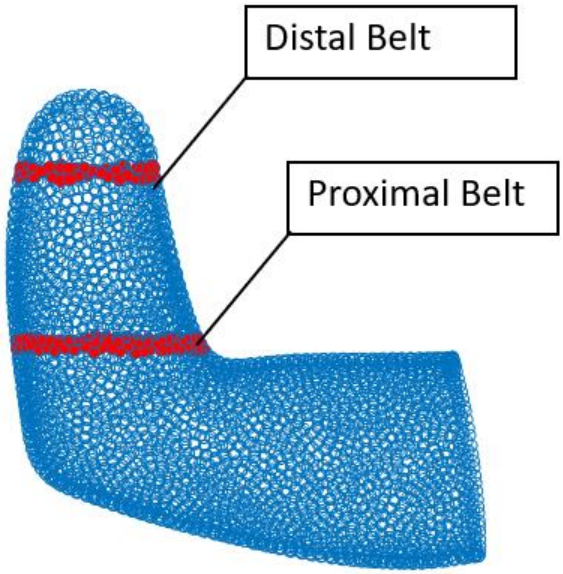

Figure 35. Landmarking the Points From the Mean Surface. Red Points Indicate the Distal Belt and the Proximal Belt

After landmark annotation of The SSM mean surface, The Statistical Shape Model is now completed and can be used for fitting a new target surface.

3.3 Statistical Shape Model Fitting

3.3.1 Overview

The main process of the automatic measurement algorithm is to recognise and indicate landmarks and other important points on the input surface. This input is a new surface which has not been marked or processed to find the correspondence in the previous steps. By using a surface that is not correlated with the SSM, we can see how well the automatic measurement algorithm performs.

3.3.2 Active Shape Model

The objective of this section is to fit the shape SSM surface into a new target by tweaking the weight of the principal components.

We used active shape model for our SSM fitting method. A new example surface **X** can be defined by transforming our statistical shape model with a certain transformation matrix **T** which consist of translation, rotation, and scaling components, together with defining the weight **b** of principal components **P**. Suppose we have a new target surface **Y**, we can fit our example model **X** to match the new target surface by minimizing the sum of square distances between corresponding model and new target surface by changing the **T** and **b** values**.** The procedure of the fitting is as follows.

1. Initialise the weight of the principal components, **b**, to zero
2. Generate the model point positions using
$$\boldsymbol{X} = \bar{\boldsymbol{x}} + \boldsymbol{P}.\boldsymbol{b}$$
3. Find the transformation matrix **T** which best align the model points **X** to the current found points **Y**
4. Project **Y** into the model coordinate frame by applying inverse of the transformation matrix
$$y = T^{-1}.Y$$
5. Project y into the tangent plane to $\bar{x}$ by scaling:
$$y' = \frac{y}{y.\bar{x}}$$
6. Update the model parameters to match to y′
$$b = P^T(y' - \bar{x})$$
7. If not converged, return to step 2.

Figure 36 shows an example result from the general SSM that was fitted into a new target surface.

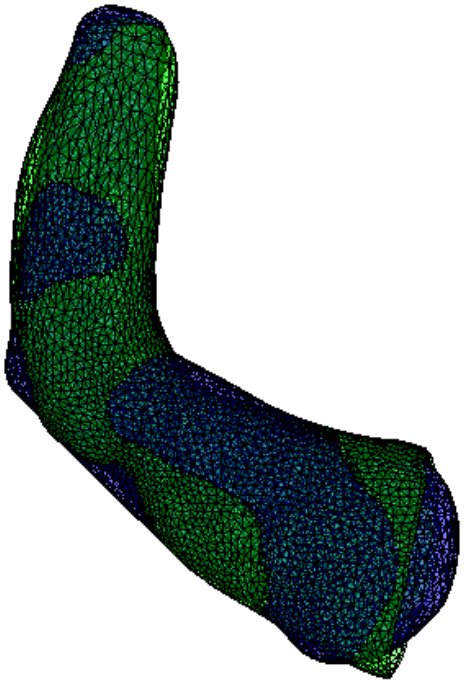

Figure 36. Result from the Active Shape Model Fitting. Mean Surface(Green) morphing to the New Target(Blue). There are still differences between two surfaces

Cootes (2000) suggested that during training the number of shape modes could be chosen so as to explain a given proportion (e.g. 98%) of the variance exhibited in the training set [44]. An alternative approach is to choose enough modes that the model can approximately any training example to within a given accuracy. For instance, we may wish that the best approximation to an example has every point within one pixel of the corresponding example points. To achieve this, we build models with increasing numbers of modes, testing the ability of each to represent the training set. We choose the first model which passes our desired criteria. We also avoid having a high number of unnecessary modes because it appears that a few modes can cause a distortion to the fitting process and result in a worse output. An example of a higher number of shape mode used that caused an abnormal shape is shown on Figure 37.

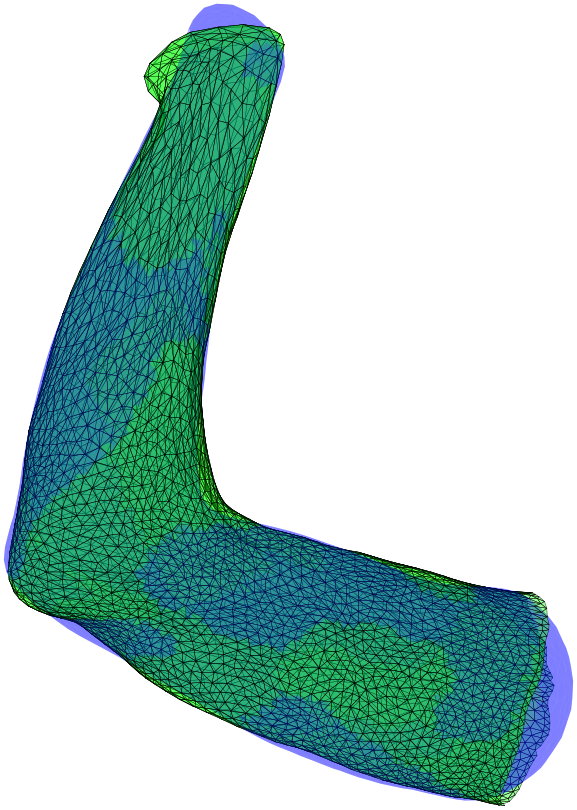

Figure 37. Excessive shape mode resulted in an abnormal shape. The tip of the stump model is not shaped like a normal stump.

3.3.3 Local Deformation

The objective of this section is to deform the fitted surface into the target to minimize errors between them.

After finding the weight of the principal components, now our fitted model has transformed into a shape which represents the new target surface within the scope of the principal components. However, there is still an apparent error between the fitted model and the new target surface. We reduced the small error by applying the Non-Rigid ICP in order to do local deformation of the surface. The fitted model in Figure 38 now has a smaller error, but still represent a valid example model.

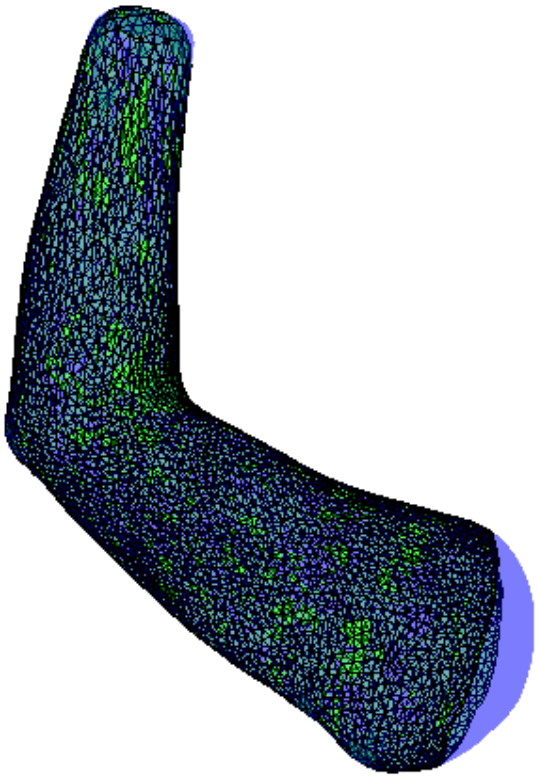

Figure 38. Further result from the Non-Rigid ICP. Mean Surface(Green) morphing to the New Target(Blue). The difference between two surface is very small compared to the previous process.

The output of the SSM fitting process is a fitted model of the new target surface with all the landmark points attached to it as shown in Figure 39.

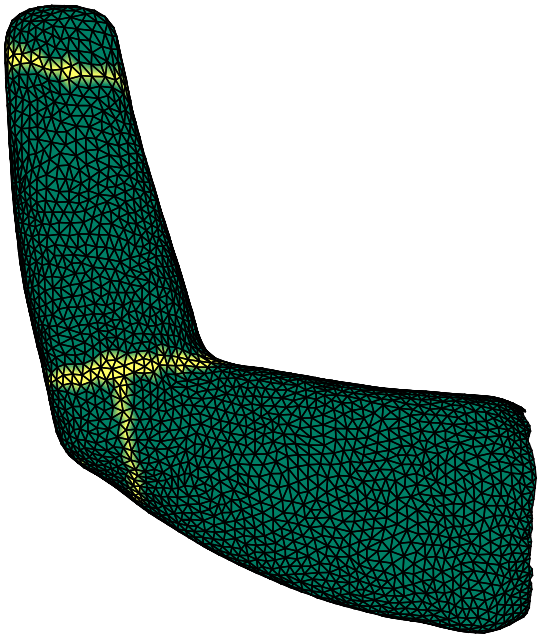

Figure 39. Final result of the Statistical Shape Model Fitting to a New Target

3.4 Measurement Method

3.4.1 Overview

Measurement can be done after the SSM is fitted into the new target. In the previous step, we pre-allocated landmark points and circumference lines in the mean surface of the SSM. Therefore, when the SSM is morphing into the new target, the final position of the pre-allocated points and lines also approximately represents the landmarks and circumferences of the new target.

3.4.2 Geodesic Distance

We measure the distance between landmarks by using a geodesic path method. From two points on the target, we find the shortest path along the surface. By this way, it can mimic the tape measurement. We used the exact geodesic code that is based on Mitchell et al.(1987) [62]. They have provided an algorithm for subdividing the surface of an arbitrary polyhedron so that the length of the shortest path from a given source point to any point on the surface may be obtained simply by locating in the subdivision.

In our algorithm, we are interested in finding the distance from the wrist points or any other cut points to the elbow points. This distance will be used for building the prosthetic socket. In Figure 40, the algorithm finds the shortest path between the cut point and the ulna point over the upper limb surface.

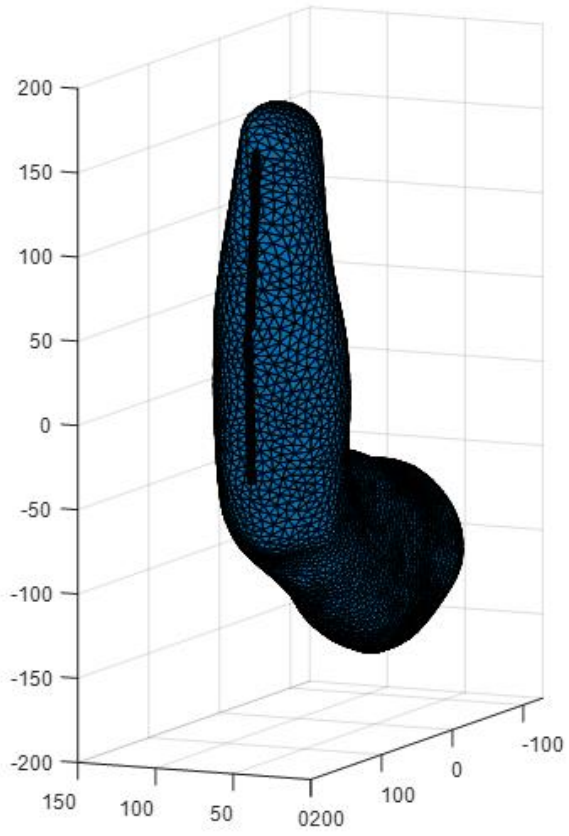

Figure 40. Geodesic Distance measurement. The thick black line indicates the geodesic line between wrist point and the ulna point of the lower arm.

3.4.3 Circumference Measurement

Circumference measurement is done by pre-allocating "belt" vertices on the SSM as shown in Figure 35. During the fitting process, the belt can morph into a new target, to find the required circumference. However, it can also pose a problem when the vertices are not aligned after the fitting process, resulting in an abnormal circumference of the upper limb. We are using an intersection line method as our main circumference measurement. We find the intersection line between a corrected regression plane and the model surface and measure the Euclidean distance of the intersection lines.

The solution of acquiring a circumference in the model from Wasenmuller (2015) is applied in our automatic measurement algorithm code to achieve a smoother belt [52]. We create a regression plane between all vertices that is normal to the arm axis. After that, we acquired the intersection line between the plane and the model surface as shown in Figure 41. To get a correct angle of plane, we improve the solution by creating an axis along the lower arm. The line is created from 2 center points of the previous intersection line. A new regression plane created from plane perpendicular from the axis as shown in Figure 42. Circumferences lines that resulted from intersection between the model and the corrected plane is shown in Figure 43. Furthermore, we determine and mark which vertices that are closest to the plane intersection (we can determine the maximum distance). After that, we calculate the Euclidean distance between all marked vertices. The final regression plane and circumference lines is shown in Figure 44.

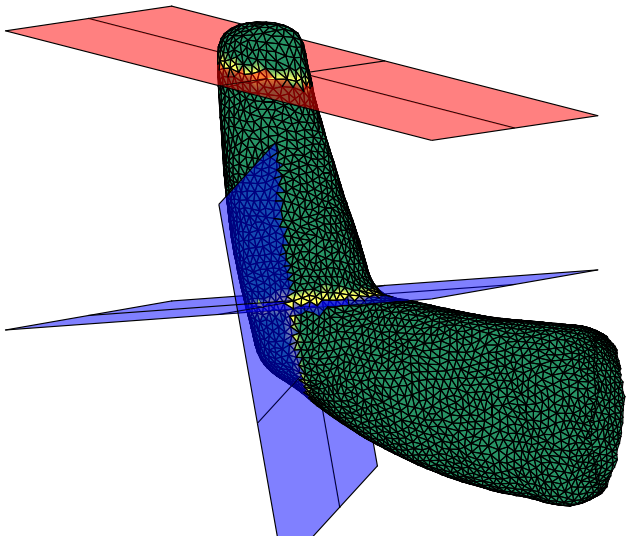

Figure 41. Fitted Surface with the Regression Plane. The Red Plane is fitted on the yellow vertices on the wrist. The Blue Plane is fitted on the yellow vertices on the elbow

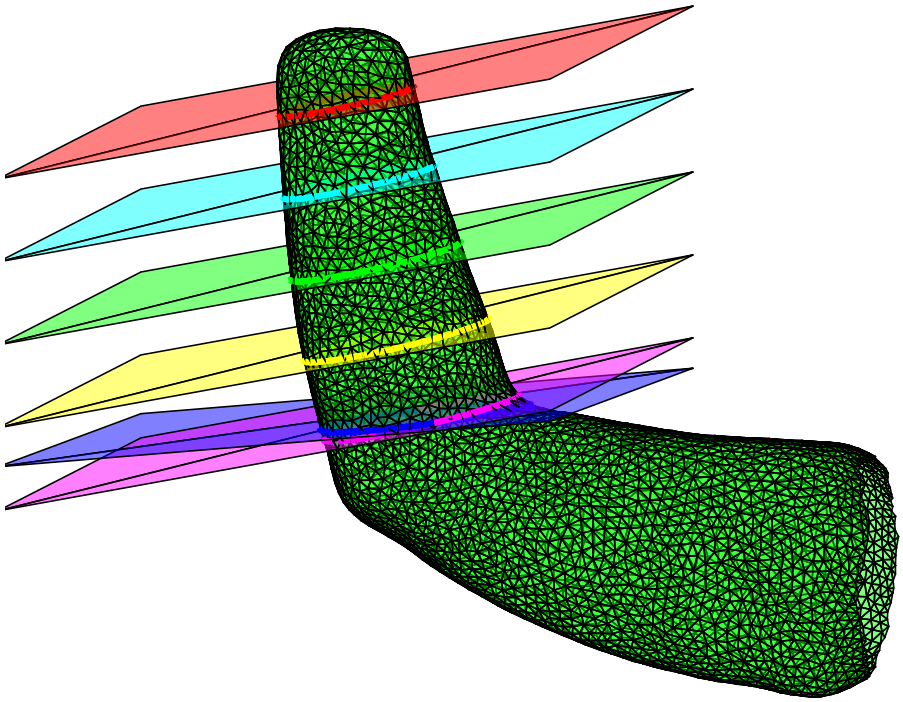

Figure 42. Corrected Plane perpendicular to lower arm axis. Red plane is corrected plane on the wrist cut. Cyan plane is 75% Cut. Green plane is 50% Cut. Yellow Plane is 25% Cut. Purple plane is corrected plane for the Proximal Belt. Blue plane is the old plane of the Proximal Belt.

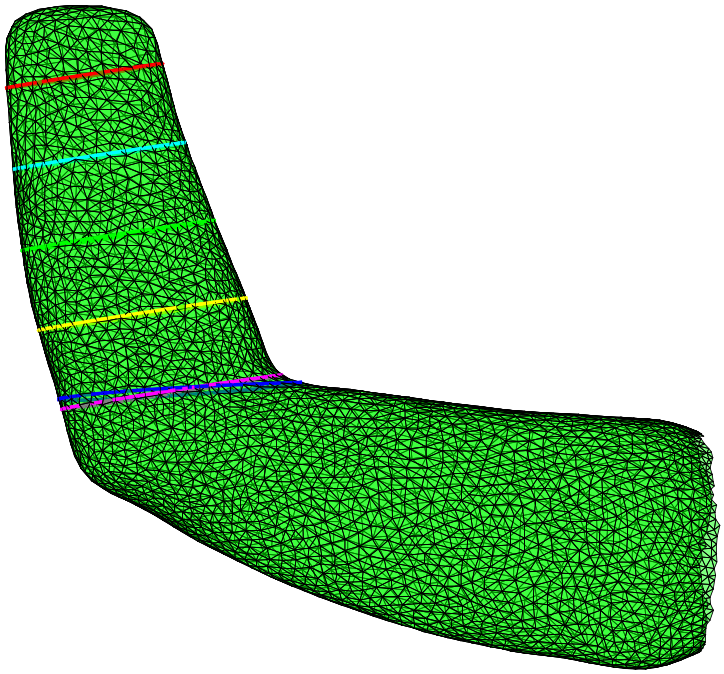

Figure 43. Circumference Lines on the Fitted Surface. Red Line indicate Distal Belt circumference. Cyan line indicate 75% circumference. Green line indicate 50% circumference. Yellow line indicate 25% circumference. Purple line indicate corrected Proximal Belt circumference. Blue line indicate second Proximal Belt circumference.

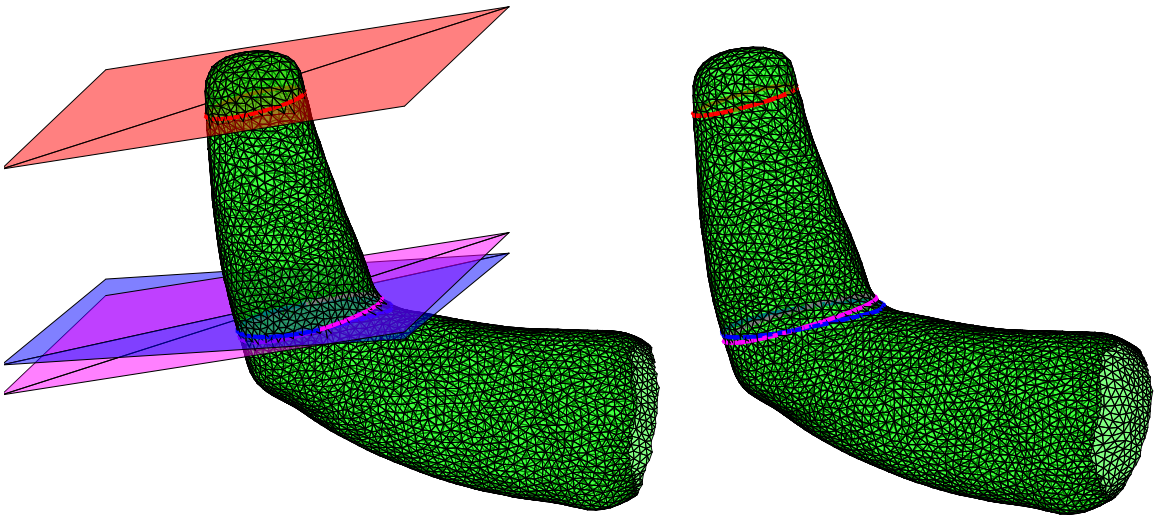

Figure 44. Intersection Planes on the Left Surface and Circumference Lines on the Right Surface.

Chapter 4: Experiment

4.1 Overview

In order to validate that our code is working with other real human models, we conduct an experiment to test the precision of our model. In this chapter, we present the experiment that was conducted at 5 September 2018 at the Faculty of Industrial Design Engineering TU Delft.

We also present the result of the experiment along with the comparison between the automatic measurement algorithm from the previous chapter. As mentioned in chapter 3, for our code we created SSMs with different training sets. For the first approach, we created SSMs that strictly contains models from a certain cut length. This means that we created an SSM exclusively for each category of cut. For example, the wrist cut 3D models is grouped as a wrist cut SSM, and this approach also applies to other cut lengths. For the second approach, we combined models with all cut length together. This means that we created an SSM with all models regardless of their cut lengths. The performances of each of the algorithm will be compared in this chapter.

4.2 Method

Our method to validate the model was to compare a real arm measurement which is regularly done by prosthetic expert and our automatic measurement algorithm with a digital 3D scanned model. The objective of this comparison is to see if our model can locate the important landmarks and girths while also providing precise measurements of the mentioned items.

The hypothesis was that the result from the specialized SSM will have a better precision compared to the second approach. However, we expected that the general SSM can provide an acceptable result without the need of having multiple different SSMs. This is also the objective of the experiment, to find out whether having a single SSM with combined cut lengths can be suitable for all different lengths of amputation. We assume that the input is ideal. Therefore, scans that produced incomplete surfaces and holes on the upper limb surface are repeated until it produced complete a surface.

In the comparison, we measure circumferences needed for making a WILMER socket for an upper limb prosthesis. We compared the two circumferences and two lines, Distal Belt, Proximal Belt, Radius Line and Ulna Line on the fitted surface with the tape measurement of the circumference.

For the scanning, we used a full body scanner 3dMD with 10 modules from Industrial Design Faculty TU Delft. After the scanning process, we also measured their hand circumferences and lengths with a measuring tape and a digital calliper. Their hands are marked with a paper foam tape to mark the points. The points are inner wrist, outer wrist, 75%, 50%, and 25% lower arm length, antecubital fossa, olecranon and ulna point. For each marked point, the circumference is measured. Later, this will emulate the lower arm amputation in different lengths.

4.3 Participants

We scanned 19 participants consist from TU Delft students and researchers with the age range of 20-37 years old. The average body mass index from the participants is 23.25. The requirement to become a subject in this experiment is that the participant need to have a healthy hand without amputation or abnormalities.

4.4 Scanning Setup

The experiment was done in the faculty of Industrial Design Engineering TU Delft. We used a full body scanner 3DMD Body System with 10 modules as shown in Figure 45. Each module is a 10Hz module based on optic system with multiple cameras to capture images which will be processed into a 3D model. We scanned the participants with their hand posing in 90^{o} bending position. The result of the scanning is a full body 3d Model as shown in Figure 46.

Furthermore, we processed the Full body model into the upper limb stump in Meshlab by segmenting it from the shoulder, and then cut the lower arm to be reconstructed with Screened Poisson surface reconstruction method, and finally the surface is uniformly re-meshed with the ACVD software. The reconstructed upper limb surface is shown in Figure 47.

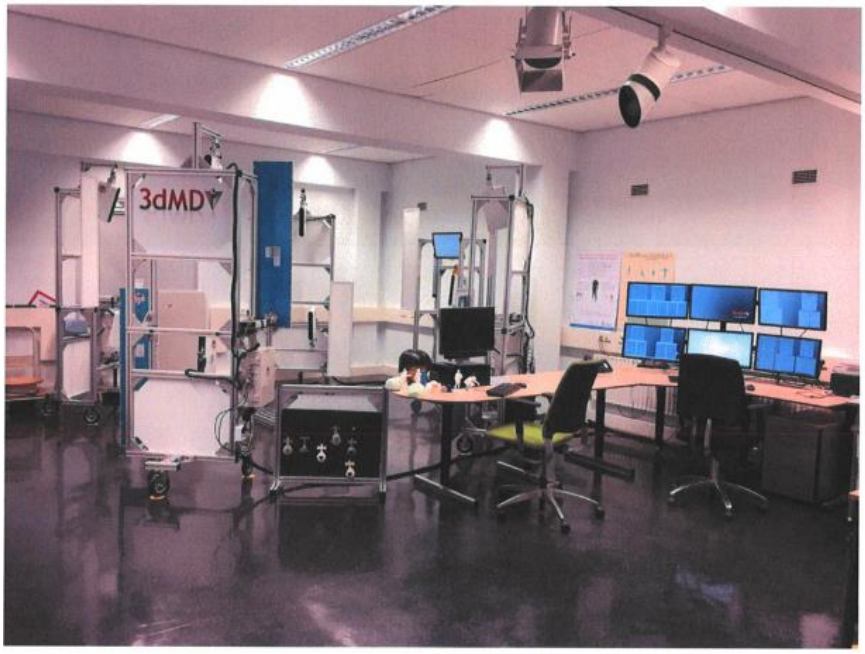

Figure 45. Scanning setup with Camera modules on the left side and working station on the right side.

Figure 46. Example of a scan result from the 3dMD full body scanner

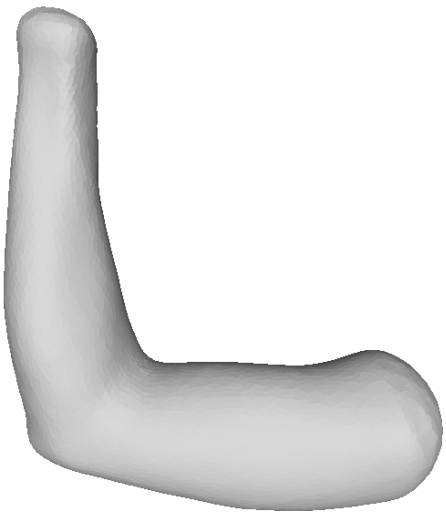

Figure 47. Reconstructed Upper limb surface from the subject scan.

4.5 Manual Measurement

We used a measuring tape to manually measure the participants. We conducted 10 Measurements of the lower arm. This includes 5 Girth Circumferences, 3 lengths, and 2 Cross section diameters. The participants were asked to pose their arm the way as they have scanned before to avoid wrong measurement. The measuring tape is calibrated first with a calliper to ensure that our measurement is valid. Our measuring tape has overestimation error of 1 mm after a calibration with the calliper.

Figure 48. Putting markers in the subject lower arm.

Figure 49. Measuring the circumference by using measuring tape.

4.6 Evaluation of Automatic Measurement

After acquiring the processed models and manual measurement numbers, we ran the automatic measurement algorithm with the processed models as the input. There are two approaches for each model. The first approach is to use the General SSM, and the second approach is to use the specialized SSM for each cut length.

We run every processed 3D surface in the MATLAB. The computing time of the code takes 35-40 seconds for each model. The results from the automatic measurement algorithm is shown in Figure 50 and Figure 51. In Figure 50 , the red line is the Distal Belt and the purple line is the Proximal Belt. In Figure 51, the black line on the left figure shows Radius Line and the black line on the right figure shows the Ulna Line

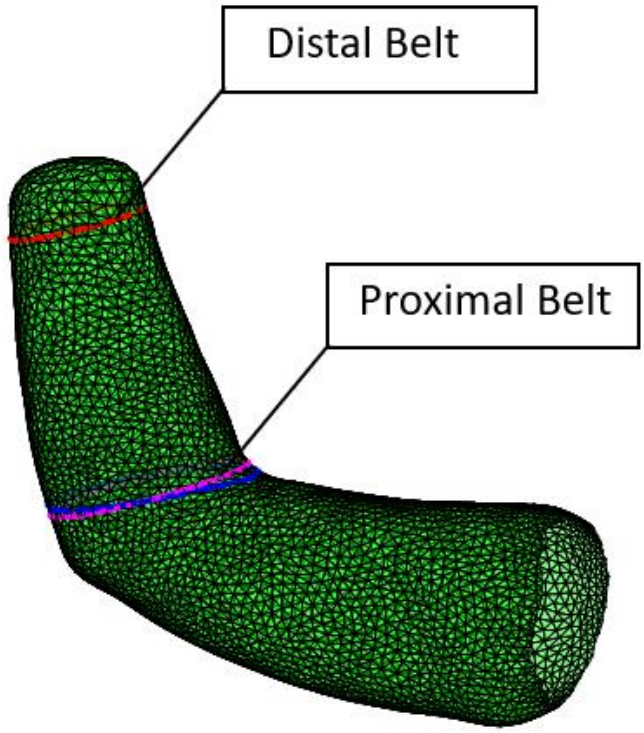

Figure 50. Circumference Lines from Automatic Measurement Algorithm. Red Line is the Distal Belt, Blue and Purple Line is the Proximal Belt.

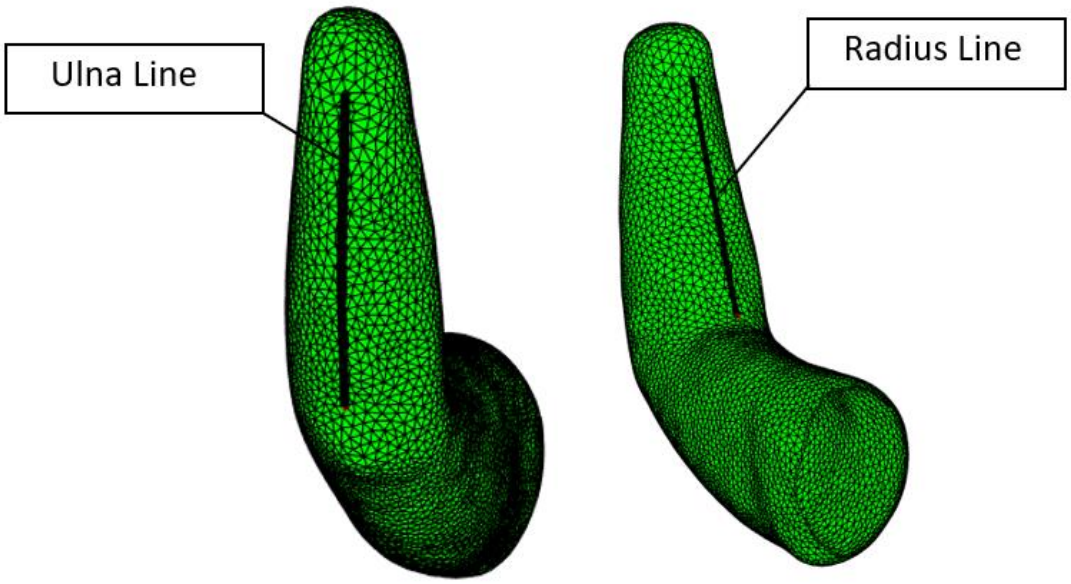

Figure 51. Geodesic Line from Automatic Measurement Algorithm. Left: Black Line showing Radius Line. Right: Black Line showing Ulna Line.

4.7 Result

The result from the automatic measurement code will be compared with the manual measurement result counterpart. We assumed that the manual measurement is the reference value and every measurement error and percentage is based on the difference of the digital measurement from the manual measurement. The locations of Distal Belt, Proximal Belt, Ulna Line, and Radius Line can be seen in previous section 4.6 in Figure 50 and Figure 51.

4.7.1 Manual Measurement

The manual measurement of circumferences, length, and cross section lines is shown in Table 1.

Table 1. Result of Manual Measurement (cm)

Subject	Circumferences (cm)					Length (cm)			Cross Section (cm)	
	Wrist (100%)	75%	50%	25%	Proximal Belt	Outside Line	Ulna Line	Radius Line	Width	Depth
1	16.2	18.4	22.8	26.6	26.4	28.5	20.6	21.2	5.2	4.3
2	15.7	19.0	23.4	25.3	25.8	26.3	20.4	21.7	5.1	3.6
3	13.5	15.7	19.5	23.0	22.8	23.3	19.5	19.7	4.7	3.2
4	14.3	16.0	19.5	22.5	23.0	24.0	20.0	20.0	5.0	3.3
5	18.4	20.0	24.3	29.8	30.0	29.7	24.4	23.5	6.2	4.8
6	15.6	17.5	21.0	24.7	24.8	25.0	21.8	21.4	5.2	3.9
7	18.2	20.5	24.7	30.0	30.2	27.7	21.7	23.5	5.9	4.9
8	16.3	18.1	21.1	26.0	26.4	28.7	22.5	21.8	5.6	4.1
9	16.4	17.1	21.0	24.3	24.7	25.5	22.2	21.7	5.2	3.6
10	15.5	17.0	21.0	25.4	26.6	25.0	20.4	20.7	5.3	3.6
11	15.6	17.8	22.3	25.8	26.4	27.0	22.0	22.1	5.4	3.8
12	15.1	15.2	18.6	24.0	25.1	24.8	20.5	20.6	5.3	3.6
13	15.5	17.6	21.5	25.2	26.1	28.3	22.8	22.8	5.6	4.1
14	15.8	17.7	21.5	25.0	26.1	25.9	19.2	19.7	5.4	4.1
15	15.9	17.6	22.3	26.3	27.3	27.8	21.8	22.5	5.3	3.9
16	15.8	15.5	19.0	23.8	25.4	25.9	20.3	21.2	5.5	3.4
17	14.2	16.4	19.4	23.5	24.2	24.7	19.9	20.4	4.9	3.5
18	15.0	16.7	20.5	25.0	26.1	24.0	18.5	19.7	5.1	3.8
19	17.4	18.6	22.0	27.2	27.8	29.6	23.8	23.6	5.7	4.3

After obtaining the raw result of manual measurement, the overall value is reduced by 0.1 cm due to the systematic error of the measurement tape. We also perform three repetitions of measurements on three subjects to measure the observer error which is shown on Table 2. From the repeated measurement, the average deviation of the circumference measurement is 0.58 cm and the average deviation of the line measurement is 0.44 cm.

Table 2. Observer error of the manual measurement. Subject 2 , Subject 3, and Subject 10 are measured 3 times.

		Circumference (cm)						Lines (cm)			
		Wrist	75%	50%	25%	Proximal Belt		Outside	Ulna	Radius	
Subject 2	**Measurement 1**	15.70	19.00	23.40	25.30	25.80		26.30	20.40	21.70	
	Measurement 2	15.40	17.10	20.50	23.60	24.90		26.80	22.70	22.50	
	Measurement 3	14.70	16.50	20.10	23.40	25.70		26.60	21.50	21.60	
	Standard Deviation	**0.42**	**1.07**	**1.47**	**0.85**	**0.40**	**0.84**	**0.21**	**0.94**	**0.40**	**0.52**
Subject 3	**Measurement 1**	13.50	15.70	19.50	23.00	22.80		23.30	19.50	19.70	
	Measurement 2	12.90	14.40	18.20	21.80	22.50		22.90	17.30	17.80	
	Measurement 3	13.00	14.40	18.50	21.20	22.60		22.70	17.70	17.70	
	Standard Deviation	**0.26**	**0.61**	**0.56**	**0.75**	**0.12**	**0.46**	**0.25**	**0.96**	**0.92**	**0.71**
Subject 10	**Measurement 1**	16.40	17.10	21.00	24.30	24.70		25.50	22.20	21.70	
	Measurement 2	14.80	16.60	20.20	23.50	23.90		25.30	21.90	21.60	
	Measurement 3	15.10	16.50	20.30	23.20	23.70		25.50	22.00	21.80	
	Standard Deviation	**0.69**	**0.26**	**0.36**	**0.46**	**0.43**	**0.44**	**0.09**	**0.12**	**0.08**	**0.10**
	Deviation Average						**0.58**				**0.44**

4.7.2 Wrist Cut

Firstly, we investigate the difference of measurement between the SSMs and the manual measurement on the wrist cut. The results of the Specialized SSM are shown in Table 3 and Table 4 while the result of the General SSM are shown in Table 5 and Table 6. The locations of Distal Belt, Proximal Belt, Ulna Line, and Radius Line can be seen in previous section 4.6 in Figure 50 and Figure 51.

Table 3. Absolute Error (cm) of Specialized SSM in Wrist Cut Measurement

Subject	**Absolute Error compared to Manual Measurement**						
	Circumferences (cm)		**Length (cm)**		**Average and Standard Deviation (cm)**		
	Distal Belt	**Proximal Belt**	**Ulna Line**	**Radius Line**	**Average**	**Average Total**	**Error STDEV**
1	0.93	1.09	0.85	0.35	**0.80**	**0.85**	0.35
2	0.81	1.37	1.21	2.71	**1.53**		
3	0.79	0.66	1.67	1.78	**1.22**		
4	0.82	0.68	0.03	0.48	**0.50**		
5	1.65	0.28	3.88	2.58	**2.10**		

6	1.12	0.33	1.03	0.01	**0.62**		
7	0.99	0.52	0.38	1.71	**0.90**		
8	0.72	0.36	0.26	1.16	**0.63**		
9	0.87	0.53	1.21	0.18	**0.70**		
10	0.99	1.44	0.59	0.30	**0.83**		
11	1.46	0.73	0.64	1.08	**0.98**		
12	0.67	1.10	0.20	0.68	**0.66**		
13	1.02	0.91	0.16	0.06	**0.54**		
14	1.00	0.58	0.33	0.15	**0.51**		
15	1.09	0.03	1.02	0.48	**0.65**		
16	0.77	0.76	1.42	1.22	**1.04**		
17	0.59	0.80	0.85	0.17	**0.60**		
18	1.11	1.02	0.88	0.26	**0.82**		
19	1.50	0.59	0.08	0.20	**0.60**		
Average	**0.99**	**0.73**	**0.88**	**0.82**			
STDEV	0.28	0.36	0.85	0.82			

Table 4. Signed Error (cm) of Specialized SSM in Wrist Cut Measurement

Subject	**Signed Error compared to Manual Measurement**						
	Circumferences (cm)		**Length (cm)**		**Average and Standard Deviation (cm)**		
	Distal Belt	**Proximal Belt**	**Ulna Line**	**Radius Line**	**Average**	**Average Total**	**Error STDEV**
1	0.93	-1.09	-0.85	0.35	**-0.16**	**0.53**	0.62
2	0.81	1.37	1.21	2.71	**1.53**		
3	0.79	0.66	1.67	1.78	**1.22**		
4	0.82	-0.68	-0.03	0.48	**0.15**		
5	1.65	0.28	3.88	2.58	**2.10**		
6	1.12	-0.33	1.03	0.01	**0.46**		
7	0.99	0.52	-0.38	1.71	**0.71**		
8	0.72	-0.36	-0.26	-1.16	**-0.27**		
9	0.87	0.53	1.21	0.18	**0.70**		
10	0.99	1.44	-0.59	0.30	**0.53**		
11	1.46	0.73	0.64	1.08	**0.98**		
12	0.67	1.10	0.20	0.68	**0.66**		
13	1.02	0.91	0.16	0.06	**0.54**		
14	1.00	0.58	-0.33	0.15	**0.35**		
15	1.09	0.03	-1.02	0.48	**0.15**		
16	0.77	-0.76	-1.42	-1.22	**-0.66**		
17	0.59	0.80	-0.85	0.17	**0.18**		
18	1.11	1.02	-0.88	0.26	**0.38**		
19	1.50	0.59	0.08	0.20	**0.60**		
Average	**0.99**	**0.39**	**0.18**	**0.57**			
STDEV	0.28	0.71	1.20	1.01			

Table 5. Absolute Error (cm) of General SSM in Wrist Cut Measurement

Subject	Absolute Error compared to Manual Measurement						
	Circumferences (cm)		Length (cm)		Average and Standard Deviation (cm)		
	Distal Belt	Proximal Belt	Ulna Line	Radius Line	Average	Average Total	Error STDEV
1	2.25	3.3	5.17	2.84	**3.39**	**3.44**	1.59
2	0.93	0.84	5.52	6.56	**3.46**		
3	2.5	0.74	5.21	5.95	**3.6**		
4	1.39	3.49	5.06	4.42	**3.59**		
5	1.35	0.35	7.52	6.15	**3.84**		
6	2.42	2.96	5.56	4.12	**3.77**		
7	1.29	0.28	5.64	6.47	**3.42**		
8	2.74	8.14	4.26	1.2	**4.09**		
9	2.5	1.7	6.19	4.38	**3.69**		
10	2.48	0.48	4.42	4.17	**2.89**		
11	2.51	2.69	5.85	4.58	**3.91**		
12	1.21	1.35	4.76	4.63	**2.99**		
13	1.77	0.87	5.28	4.93	**3.21**		
14	3.72	1.28	4.15	4.33	**3.37**		
15	3.12	5.32	4.39	1.65	**3.62**		
16	0.27	3.67	3.1	2.25	**2.32**		
17	4.11	2.48	3.96	2.37	**3.23**		
18	2.38	1.11	3.86	4.53	**2.97**		
19	1.6	5.41	5.79	3.59	**4.1**		
Average	**2.13**	**2.44**	**5.04**	**4.16**			
STDEV	0.93	2.04	0.98	1.51			

Table 6. Signed Error (cm) of Generalized SSM in Wrist Cut Measurement

	Signed Error compared to Manual Measurement						
	Circumferences (cm)		Length (cm)		Average and Standard Deviation (cm)		
Subject	Distal Belt	Proximal Belt	Ulna Line	Radius Line	Average	Average Total	Error STDEV
1	-2.25	-5.10	5.17	2.84	**0.16**	**1.13**	0.93
2	-0.93	0.84	5.52	6.56	**3.00**		
3	-2.50	-0.74	5.21	5.95	**1.98**		
4	-1.39	-3.49	5.06	4.42	**1.15**		
5	-1.35	0.35	7.52	6.15	**3.17**		
6	-2.42	-2.96	5.56	4.12	**1.08**		
7	-1.29	0.28	5.64	6.47	**2.78**		
8	-2.74	-8.14	4.26	1.20	**-1.36**		
9	-2.50	-1.70	6.19	4.38	**1.59**		
10	-2.48	0.48	4.42	4.17	**1.65**		
11	-2.51	-2.69	5.85	4.58	**1.31**		
12	-1.21	-1.35	4.76	4.63	**1.71**		
13	-1.77	-0.87	5.28	4.93	**1.89**		
14	-3.72	-1.28	4.15	4.33	**0.87**		

15	-3.12	-7.12	4.39	1.65	**-1.05**		
16	-0.27	-4.88	3.10	2.25	**0.05**		
17	-4.11	-3.81	3.96	2.37	**-0.40**		
18	-2.38	-1.11	3.86	4.53	**1.23**		
19	-1.60	-5.41	5.79	3.59	**0.59**		
Average	**-2.13**	**-2.56**	**5.04**	**4.16**			
STDEV	0.93	2.56	0.98	1.51			

4.7.3 75% Cut

For 75% Cut measurements, the results of the Specialized SSM are shown in Table 7 and Table 8 while the results of the General SSM are shown in Table 9 and Table 10. The locations of Distal Belt, Proximal Belt, Ulna Line, and Radius Line can be seen in previous section 4.6 in Figure 50 and Figure 51.

Table 7. Absolute Error (cm) of Specialized SSM in 75% Cut Measurement

Subject	**Absolute Error compared to Manual Measurement**						
	Circumferences (cm)		**Length (cm)**		**Average and Standard Deviation (cm)**		
	75%	**Proximal Belt**	**Ulna Line**	**Radius Line**	**Average**	**Average Total**	**Error STDEV**
1	1.52	1.13	0.63	0.23	**0.88**	**0.87**	0.50
2	1.90	0.99	0.27	1.12	**1.07**		
3	0.72	0.67	1.80	2.36	**1.39**		
4	1.22	0.82	0.43	0.80	**0.82**		
5	0.65	0.35	2.59	2.51	**1.52**		
6	0.04	0.40	0.62	0.97	**0.50**		
7	1.40	0.36	0.25	2.44	**1.11**		
8	0.06	2.01	0.94	1.08	**1.02**		
9	0.40	0.32	0.97	1.03	**0.68**		
10	0.01	1.31	0.02	0.95	**0.58**		
11	0.68	0.90	1.54	2.16	**1.32**		
12	0.26	0.87	0.96	1.40	**0.87**		
13	0.75	0.84	0.84	1.29	**0.93**		
14	0.05	0.81	0.00	0.83	**0.42**		
15	0.41	1.21	1.35	0.37	**0.84**		
16	0.36	1.00	1.57	0.59	**0.88**		
17	0.23	0.05	0.78	0.02	**0.27**		
18	0.61	1.23	0.68	0.58	**0.77**		
19	0.44	0.48	0.73	1.01	**0.67**		
Average	**0.62**	**0.83**	**0.89**	**1.14**			
STDEV	0.53	0.44	0.63	0.72			

Table 8. Signed Error (cm) of Specialized SSM in 75% Cut Measurement

Subject	**Signed Error compared to Manual Measurement**						
	Circumferences (cm)		**Length (cm)**		**Average and Standard Deviation (cm)**		
	Distal Belt	**Proximal Belt**	**Ulna Line**	**Radius Line**	**Average**	**Average Total**	**Error STDEV**
1	1.52	-1.13	-0.63	0.23	**0.00**	**0.47**	0.96
2	1.90	0.99	-0.27	1.12	**0.93**		

3	0.72	0.67	1.80	2.36	**1.39**		
4	1.22	-0.82	0.43	0.80	**0.41**		
5	0.65	0.35	2.59	2.51	**1.52**		
6	-0.04	-0.40	0.62	0.97	**0.29**		
7	1.40	0.36	0.25	2.44	**1.11**		
8	0.06	-2.01	-0.94	-1.08	**-0.99**		
9	0.40	0.32	0.97	1.03	**0.68**		
10	0.01	1.31	-0.02	0.95	**0.57**		
11	0.68	0.90	1.54	2.16	**1.32**		
12	-0.26	0.87	0.96	1.40	**0.74**		
13	0.75	0.84	0.84	1.29	**0.93**		
14	-0.05	0.81	0.00	0.83	**0.40**		
15	0.41	-1.21	-1.35	-0.37	**-0.63**		
16	0.36	-1.00	-1.57	-0.59	**-0.70**		
17	0.23	0.05	-0.78	-0.02	**-0.13**		
18	0.61	1.23	-0.68	0.58	**0.43**		
19	0.44	0.48	0.73	1.01	**0.67**		
Average	**0.58**	**0.14**	**0.24**	**0.93**			
STDEV	0.57	0.93	1.07	0.98			

Table 9. Absolute Error (cm) of General SSM in 75% Cut Measurement

Subject	**Absolute Error compared to Manual Measurement**						
	Circumferences (cm)		**Length (cm)**		**Average and Standard Deviation (cm)**		
	75%	**Proximal Belt**	**Ulna Line**	**Radius Line**	**Average**	**Average Total**	**Error STDEV**
1	2.64	5.37	2.6	3.45	**3.51**	**2.97**	1.69
2	1.6	0.36	2.61	3.84	**2.1**		
3	2.71	0.95	3.83	4.24	**2.94**		
4	1.71	4.02	2.06	2.35	**2.53**		
5	2.73	0.31	5.05	4.74	**3.21**		
6	3.15	3.68	3.68	3.71	**3.55**		
7	1.62	0.1	2.67	4.39	**2.2**		
8	3.79	6.82	0.45	0.89	**2.99**		
9	3.59	1.87	3.59	3.64	**3.17**		
10	3.72	0.29	2.54	3.14	**2.42**		
11	3.69	2.99	3.31	3.64	**3.41**		
12	4.18	0.99	3.25	3.62	**3.01**		
13	2.32	2.36	2.81	3.02	**2.63**		
14	4.52	1.09	2.18	2.92	**2.68**		
15	5.05	6.02	0.79	2.03	**3.47**		
16	3.08	5.85	1.81	2.75	**3.37**		
17	3.95	3.02	1.18	2.21	**2.59**		
18	3.51	1.19	2.11	3.33	**2.53**		
19	3.52	5.22	3.61	3.8	**4.04**		
Average	**3.21**	**2.76**	**2.64**	**3.25**			
STDEV	0.94	2.17	1.10	0.89			

Table 10. Signed Error (cm) of Generalized SSM in 75% Cut Measurement

Subject	Signed Error compared to Manual Measurement						
	Circumferences (cm)		Length (cm)		Average and Standard Deviation (cm)		
	Distal Belt	Proximal Belt	Ulna Line	Radius Line	Average	Average Total	Error STDEV
1	-2.64	5.37	2.60	3.45	**2.19**	**1.36**	0.94
2	-1.60	0.36	2.61	3.84	**1.30**		
3	-2.71	0.95	3.83	4.24	**1.58**		
4	-1.71	4.02	2.06	2.35	**1.68**		
5	-2.73	0.31	5.05	4.74	**1.85**		
6	-3.15	3.68	3.68	3.71	**1.98**		
7	-1.62	0.10	2.67	4.39	**1.39**		
8	-3.79	6.82	0.45	0.89	**1.09**		
9	-3.59	1.87	3.59	3.64	**1.38**		
10	-3.72	0.29	2.54	3.14	**0.56**		
11	-3.69	2.99	3.31	3.64	**1.56**		
12	-4.18	0.99	3.25	3.62	**0.92**		
13	-2.32	2.36	2.81	3.02	**1.47**		
14	-4.52	1.09	2.18	2.92	**0.42**		
15	-5.05	6.02	0.79	2.03	**0.95**		
16	-3.08	5.85	1.81	2.75	**1.83**		
17	-3.95	3.02	1.18	2.21	**0.62**		
18	-3.51	1.19	2.11	3.33	**0.78**		
19	-3.52	5.22	3.61	3.80	**2.28**		
Average	**-3.21**	**2.76**	**2.64**	**3.25**			
STDEV	0.94	2.17	1.10	0.89			

4.7.4 50% Cut

For 50% measurements, the results of the Specialized SSM are shown in Table 11 and Table 12 while The result of the General SSM is shown in Table 13 and Table 14. The locations of Distal Belt, Proximal Belt, Ulna Line, and Radius Line can be seen in previous section 4.6 in Figure 50 and Figure 51.

Table 11. Absolute Error (cm) of Specialized SSM in 50% Cut Measurement

Subject	Absolute Error compared to Manual Measurement						
	Circumferences (cm)		Length (cm)		Average and Standard Deviation (cm)		
	50%	Proximal Belt	Ulna Line	Radius Line	Average	Average Total	Error STDEV
1	0.53	0.72	0.40	0.35	**0.50**	**1.04**	0.69
2	0.29	0.91	0.65	1.64	**0.87**		
3	0.56	0.43	1.48	1.81	**1.07**		
4	0.60	1.38	0.43	0.75	**0.79**		
5	0.73	0.68	2.06	2.12	**1.40**		
6	0.89	1.36	1.11	1.38	**1.19**		
7	0.53	0.00	1.70	2.88	**1.28**		

8	1.59	0.29	0.92	0.66	**0.87**		
9	0.91	0.27	1.62	1.60	**1.10**		
10	1.53	1.38	0.99	1.50	**1.35**		
11	0.34	0.26	0.92	1.42	**0.73**		
12	2.43	0.73	0.71	1.09	**1.24**		
13	0.06	0.76	0.92	1.36	**0.78**		
14	1.93	0.72	0.28	0.84	**0.94**		
15	0.87	2.87	1.38	0.60	**1.43**		
16	1.14	2.44	1.01	0.15	**1.19**		
17	2.08	1.15	0.90	0.26	**1.10**		
18	1.32	1.12	0.63	1.67	**1.18**		
19	2.17	0.66	0.17	0.37	**0.84**		
Average	**1.08**	**0.95**	**0.96**	**1.18**			
STDEV	0.68	0.70	0.49	0.70			

Table 12. Signed Error (cm) of Specialized SSM in 50% Cut Measurement

Subject	**Signed Error compared to Manual Measurement**						
	Circumferences (cm)		**Length (cm)**		**Average and Standard Deviation (cm)**		
	Distal Belt	**Proximal Belt**	**Ulna Line**	**Radius Line**	**Average**	**Average Total**	**Error STDEV**
1	0.53	0.14	-0.40	0.35	**0.16**	**0.11**	1.23
2	-0.29	0.91	0.65	1.64	**0.73**		
3	-0.56	0.43	1.48	1.81	**0.79**		
4	0.60	-1.38	0.43	0.75	**0.10**		
5	-0.73	0.68	2.06	2.12	**1.04**		
6	-0.89	-1.36	1.11	1.38	**0.06**		
7	-0.53	0.00	1.70	2.88	**1.01**		
8	-1.59	0.53	-0.92	-0.66	**-0.66**		
9	-0.91	0.27	1.62	1.60	**0.65**		
10	-1.53	1.38	0.99	1.50	**0.59**		
11	-0.34	0.26	0.92	1.42	**0.56**		
12	-2.43	0.73	0.71	1.09	**0.03**		
13	0.06	0.76	0.92	1.36	**0.78**		
14	-1.93	0.72	0.28	0.84	**-0.02**		
15	-0.87	-2.87	-1.38	-0.60	**-1.43**		
16	-1.14	-2.44	-1.01	-0.15	**-1.19**		
17	-2.08	-1.15	-0.90	-0.26	**-1.10**		
18	-1.32	1.12	0.63	1.67	**0.52**		
19	-2.17	-0.66	0.17	0.37	**-0.57**		
Average	**-0.95**	**-0.10**	**0.48**	**1.01**			
STDEV	0.85	1.17	0.97	0.93			

Table 13. Absolute Error (cm) of General SSM in 50% Cut Measurement

Subject	**Absolute Error compared to Manual Measurement**						
	Circumferences (cm)		**Length (cm)**		**Average and Standard Deviation (cm)**		
	50%	**Proximal Belt**	**Ulna Line**	**Radius Line**	**Average**	**Average Total**	**Error STDEV**
1	1.16	5.92	0.2	0.4	**1.92**	**1.64**	1.67

2	1.61	0.32	0.39	1.28	**0.9**		
3	1.27	0.58	1.27	1.72	**1.21**		
4	0.73	3.44	0.49	0.79	**1.36**		
5	1.14	0.32	1.2	1.37	**1.01**		
6	1.43	4.25	0.19	0.46	**1.58**		
7	0.85	0.07	1.47	2.84	**1.31**		
8	4.39	4.7	1.97	1.08	**3.03**		
9	1.97	1.74	0.62	0.73	**1.27**		
10	2.21	0.61	0.31	0.92	**1.01**		
11	1.61	3.26	1.6	1.96	**2.11**		
12	3.37	1.1	0.66	0.99	**1.53**		
13	1.12	2.86	0.55	0.82	**1.34**		
14	2.6	0.74	0.67	0.01	**1**		
15	3.32	4.97	1.75	0.49	**2.64**		
16	2.73	6.7	1.02	0.27	**2.68**		
17	3.35	2.04	1.53	0.38	**1.83**		
18	2.21	0.56	0.43	1.37	**1.14**		
19	3.67	5.09	0.07	0.3	**2.28**		
Average	**2.14**	**2.59**	**0.86**	**0.96**			
STDEV	1.05	2.1	0.57	0.67			

Table 14. Signed Error (cm) of General SSM in 50% Cut Measurement

Subject	**Signed Error compared to Manual Measurement**						
	Circumferences (cm)		**Length (cm)**		**Average and Standard Deviation (cm)**		
	Distal Belt	**Proximal Belt**	**Ulna Line**	**Radius Line**	**Average**	**Average Total**	**Error STDEV**
1	-1.16	-5.92	10.10	7.30	**2.58**	**4.02**	1.05
2	-1.61	-0.32	10.59	11.18	**4.96**		
3	-1.27	-0.58	11.02	10.99	**5.04**		
4	-0.73	-3.44	10.49	9.46	**3.95**		
5	-1.14	0.32	13.40	12.86	**6.36**		
6	-1.43	-4.25	11.09	9.40	**3.70**		
7	-0.85	0.07	12.32	13.57	**6.28**		
8	-4.39	-4.70	9.28	7.84	**2.01**		
9	-1.97	-1.74	11.72	11.22	**4.81**		
10	-2.21	0.61	10.51	10.05	**4.74**		
11	-1.61	-3.26	12.60	10.57	**4.58**		
12	-3.37	-1.10	10.91	10.74	**4.29**		
13	-1.12	-2.86	11.95	10.61	**4.65**		
14	-2.60	-0.74	8.93	9.40	**3.75**		
15	-3.32	-4.97	9.15	8.54	**2.35**		
16	-2.73	-6.70	9.13	8.50	**2.05**		
17	-3.35	-2.04	8.42	7.62	**2.66**		
18	-2.21	-0.56	9.68	10.29	**4.30**		
19	-3.67	-5.09	11.83	9.96	**3.26**		
Average	**-2.14**	**-2.49**	**10.69**	**10.01**			
STDEV	1.05	2.22	1.35	1.61			

4.7.5 25% Cut

For 25% measurements, the results of the Specialized SSM are shown in Table 15 and Table 16 while

the results of the General SSM are shown in Table 17 and Table 18. The locations of Distal Belt, Proximal Belt, Ulna Line, and Radius Line can be seen in previous section 4.6 in Figure 50 and Figure 51.

Table 15. Absolute Error (cm) of Specialized SSM in 25% Cut Measurement

Subject	Absolute Error compared to Manual Measurement						
	Circumferences (cm)		Length (cm)		Average and Standard Deviation (cm)		
	25%	Proximal Belt	Ulna Line	Radius Line	Average	Average Total	Error STDEV
1	0.34	0.92	0.38	0.89	**0.64**	**0.96**	0.38
2	0.30	1.08	1.11	1.83	**1.08**		
3	0.54	0.56	1.54	1.85	**1.12**		
4	0.07	0.18	1.06	1.37	**0.67**		
5	0.85	0.54	1.76	1.97	**1.28**		
6	0.27	0.40	1.60	1.82	**1.02**		
7	0.44	0.15	1.85	2.63	**1.27**		
8	0.13	1.49	0.45	0.77	**0.71**		
9	0.23	0.74	1.72	1.83	**1.13**		
10	0.49	1.46	1.43	1.79	**1.30**		
11	0.43	0.64	1.59	2.00	**1.16**		
12	0.20	1.30	1.41	1.76	**1.17**		
13	0.71	0.97	1.31	1.74	**1.18**		
14	0.48	0.83	0.93	1.41	**0.91**		
15	0.19	0.46	0.07	0.57	**0.32**		
16	0.21	0.54	0.54	1.15	**0.61**		
17	0.47	0.78	0.61	1.15	**0.75**		
18	0.16	1.20	0.93	1.62	**0.98**		
19	0.19	1.00	1.04	1.46	**0.92**		
Average	**0.35**	**0.80**	**1.12**	**1.56**			
STDEV	0.20	0.38	0.51	0.48			

Table 16. Signed Error (cm) of Specialized SSM in 25% Cut Measurement

Subject	Signed Error compared to Manual Measurement						
	Circumferences (cm)		Length (cm)		Average and Standard Deviation (cm)		
	Distal Belt	Proximal Belt	Ulna Line	Radius Line	Average	Average Total	Error STDEV
1	0.34	-0.92	0.38	0.89	**0.17**	**0.82**	0.79
2	-0.30	1.08	1.11	1.83	**0.93**		
3	0.54	0.56	1.54	1.85	**1.12**		
4	-0.07	-0.18	1.06	1.37	**0.54**		
5	0.85	0.54	1.76	1.97	**1.28**		
6	0.27	-0.40	1.60	1.82	**0.82**		
7	0.44	0.15	1.85	2.63	**1.27**		
8	0.13	-1.49	0.45	0.77	**-0.03**		
9	0.23	0.74	1.72	1.83	**1.13**		
10	0.49	1.46	1.43	1.79	**1.30**		
11	0.43	0.64	1.59	2.00	**1.16**		
12	0.20	1.30	1.41	1.76	**1.17**		
13	0.71	0.97	1.31	1.74	**1.18**		

14	-0.48	0.83	0.93	1.41	**0.67**		
15	-0.19	-0.46	-0.07	0.57	**-0.04**		
16	-0.21	-0.54	0.54	1.15	**0.23**		
17	0.47	0.78	0.61	1.15	**0.75**		
18	-0.16	1.20	0.93	1.62	**0.90**		
19	0.19	1.00	1.04	1.46	**0.92**		
Average	**0.20**	**0.38**	**1.11**	**1.56**			
STDEV	0.35	0.80	0.52	0.48			

Table 17. Absolute Error (cm) of General SSM in 25% Cut Measurement

Subject	**Absolute Error compared to Manual Measurement**						
	Circumferences (cm)		**Length (cm)**		**Average and Standard Deviation (cm)**		
	25%	**Proximal Belt**	**Ulna Line**	**Radius Line**	**Average**	**Average Total**	**Error STDEV**
1	0.12	7.12	3.78	3.11	**3.53**	**2.03**	1.53
2	1.06	0.16	2.07	1.45	**1.19**		
3	0.86	1.17	1.10	0.64	**0.94**		
4	0.53	3.12	1.94	1.53	**1.78**		
5	3.86	0.17	0.80	0.59	**1.35**		
6	1.45	4.21	2.35	2.00	**2.50**		
7	4.03	0.35	0.99	0.04	**1.35**		
8	1.80	3.90	5.86	4.80	**4.09**		
9	0.10	2.12	1.63	1.40	**1.31**		
10	1.37	0.44	1.68	1.15	**1.16**		
11	2.18	2.35	1.85	1.41	**1.94**		
12	1.09	1.23	2.14	1.82	**1.57**		
13	1.38	1.76	2.49	2.22	**1.96**		
14	0.64	0.17	3.25	2.58	**1.66**		
15	1.50	3.95	5.02	3.89	**3.59**		
16	0.93	3.75	3.38	2.39	**2.61**		
17	0.81	1.05	4.03	3.00	**2.22**		
18	0.79	0.69	2.33	1.52	**1.33**		
19	0.42	2.39	3.90	3.00	**2.43**		
Average	**1.31**	**2.11**	**2.66**	**2.03**			
STDEV	0.47	0.49	0.85	0.94			

Table 18. Signed Error (cm) of General SSM in Wrist Cut Measurement

Subject	**Signed Error compared to Manual Measurement**						
	Circumferences (cm)		**Length (cm)**		**Average and Standard Deviation (cm)**		
	Distal Belt	**Proximal Belt**	**Ulna Line**	**Radius Line**	**Average**	**Average Total**	**Error STDEV**
1	0.12	-7.12	11.67	9.87	**3.63**	**6.17**	2.19
2	1.06	-0.16	13.23	14.46	**7.15**		
3	0.86	-1.17	13.53	13.21	**6.61**		
4	0.53	-3.12	13.06	12.28	**5.69**		
5	3.86	-0.17	17.50	15.89	**9.27**		
6	1.45	-4.21	14.00	12.38	**5.91**		
7	4.03	-0.35	15.29	16.93	**8.97**		

8	-1.80	-3.90	11.02	10.64	**3.99**		
9	0.10	-2.12	15.02	14.00	**6.75**		
10	1.37	0.44	13.62	13.53	**7.24**		
11	2.18	-2.35	14.65	13.69	**7.04**		
12	1.09	-1.23	13.23	13.15	**6.56**		
13	1.38	-1.76	14.61	14.05	**7.07**		
14	-0.64	-0.17	11.15	11.29	**5.41**		
15	-1.50	-3.95	11.33	11.10	**4.24**		
16	-0.93	-3.75	11.85	11.79	**4.74**		
17	-0.81	-1.05	10.89	10.65	**4.92**		
18	0.79	-0.69	11.55	11.83	**5.87**		
19	-0.42	-2.39	13.95	13.32	**6.11**		
Average	**0.67**	**-2.06**	**13.22**	**12.85**			
STDEV	1.54	1.86	1.72	1.77			

4.7.6 Cross Section Lines

The cross section line absolute and signed error of the Specialized and General SSM are shown in Table 19 and Table 20.

Table 19. Absolute Error (cm) of Specialized and General SSM in Cross Section Measurement

Subject	**Cross Section Absolute Error (cm)**			
	Specialized SSM		**General SSM**	
	Width	**Depth**	**Width**	**Depth**
1	0.19	0.10	3.39	1.92
2	0.17	0.36	0.81	0.49
3	1.06	1.21	0.70	1.59
4	0.03	0.82	2.13	1.11
5	0.27	0.36	2.95	0.01
6	0.11	0.35	3.84	0.81
7	0.05	0.29	2.94	1.42
8	0.32	0.61	5.66	3.54
9	0.09	0.54	4.10	0.05
10	0.09	0.80	3.44	0.29
11	0.47	0.58	2.57	0.78
12	0.17	0.65	1.71	0.21
13	0.51	0.49	3.68	1.40
14	0.18	0.23	2.62	0.62
15	0.14	0.07	5.57	2.57
16	0.53	1.29	3.57	3.23
17	0.03	0.03	2.73	0.90
18	0.07	0.04	2.68	0.27
19	0.14	0.06	4.64	2.30
Average	**0.24**	**0.47**	**3.15**	**1.24**
STDEV	0.25	0.36	1.30	1.03

Table 20. Signed Error (cm) of Specialized and General SSM in Wrist Cut Measurement

Subject	Cross Section Signed Error (cm)			
	Specialized SSM		General SSM	
	Width	Depth	Width	Depth
1	-0.19	-0.10	3.39	1.92
2	0.17	0.36	0.81	-0.49
3	-1.06	1.21	0.70	-1.59
4	-0.03	0.82	2.13	1.11
5	-0.27	-0.36	2.95	0.01
6	-0.11	0.35	3.84	0.81
7	0.05	-0.29	2.94	-1.42
8	-0.32	0.61	5.66	3.54
9	-0.09	0.54	4.10	0.05
10	0.09	0.80	3.44	-0.29
11	-0.47	0.58	2.57	0.78
12	-0.17	0.65	1.71	0.21
13	-0.51	0.49	3.68	1.40
14	-0.18	-0.23	2.62	-0.62
15	0.14	-0.07	5.57	2.57
16	0.53	1.29	3.57	3.23
17	0.03	-0.03	2.73	0.90
18	-0.07	-0.04	2.68	-0.27
19	-0.14	-0.06	4.64	2.30
AVG	**-0.14**	**0.34**	**3.15**	**0.75**
STDEV	0.32	0.48	1.30	1.43

4.7.7 Circumference and Length Comparison

In this section, we present the comparison of average absolute error between General and Specialized SSM in all target categories. The error comparison is shown on Table 21 and Figure 52. The Signed Error comparison is shown in Table 22.

Table 21. Absolute Error Comparison Between General and Specialized SSM in All Targets

	Target	Distal Belt	Proximal belt	Average	Target	Ulna Line	Radius Line	Average	Total Average
Specialized SSM Average Error (cm)	**Wrist Cut**	0.99	0.73	0.86	**Wrist Cut**	0.88	0.82	0.85	
	75% Cut	0.62	0.83	0.73	**75% Cut**	0.89	1.14	1.02	
	50% Cut	1.08	0.95	1.02	**50% Cut**	0.96	1.18	1.07	
	25% Cut	0.35	0.80	0.58	**25% Cut**	1.12	1.56	1.34	
	Average	0.76	0.83			0.96	1.18		0.93
Generalized SSM Average Error (cm)	**Wrist Cut**	2.13	2.44	2.29	**Wrist Cut**	5.04	4.16	4.60	
	75% Cut	3.21	2.76	2.99	**75% Cut**	2.64	3.25	2.95	
	50% Cut	2.14	2.59	2.37	**50% Cut**	0.86	0.96	0.91	
	25% Cut	1.31	2.11	1.71	**25% Cut**	2.66	2.03	2.35	
	Average	2.19	2.47			2.8	2.6		2.52

Table 22. Signed Error Comparison Between General and Specialized SSM in All Targets. Positive value indicates underestimation and negative value indicates overestimation.

	Target	Distal Belt	Proximal Belt	Ulna Line	Radius Line
Specialized SSM	**Wrist Cut**	0.99	0.39	0.18	0.57
	75% Cut	0.58	0.14	0.24	0.93
	50% Cut	-0.95	-0.1	0.48	1.01
	25% Cut	0.2	0.38	1.11	1.56
Generalized SSM	**Wrist Cut**	-2.13	-2.56	5.04	4.16
	75% Cut	-3.21	2.76	2.64	3.25
	50% Cut	-2.14	-2.49	10.69	10.01
	25% Cut	0.67	-2.06	13.22	12.85

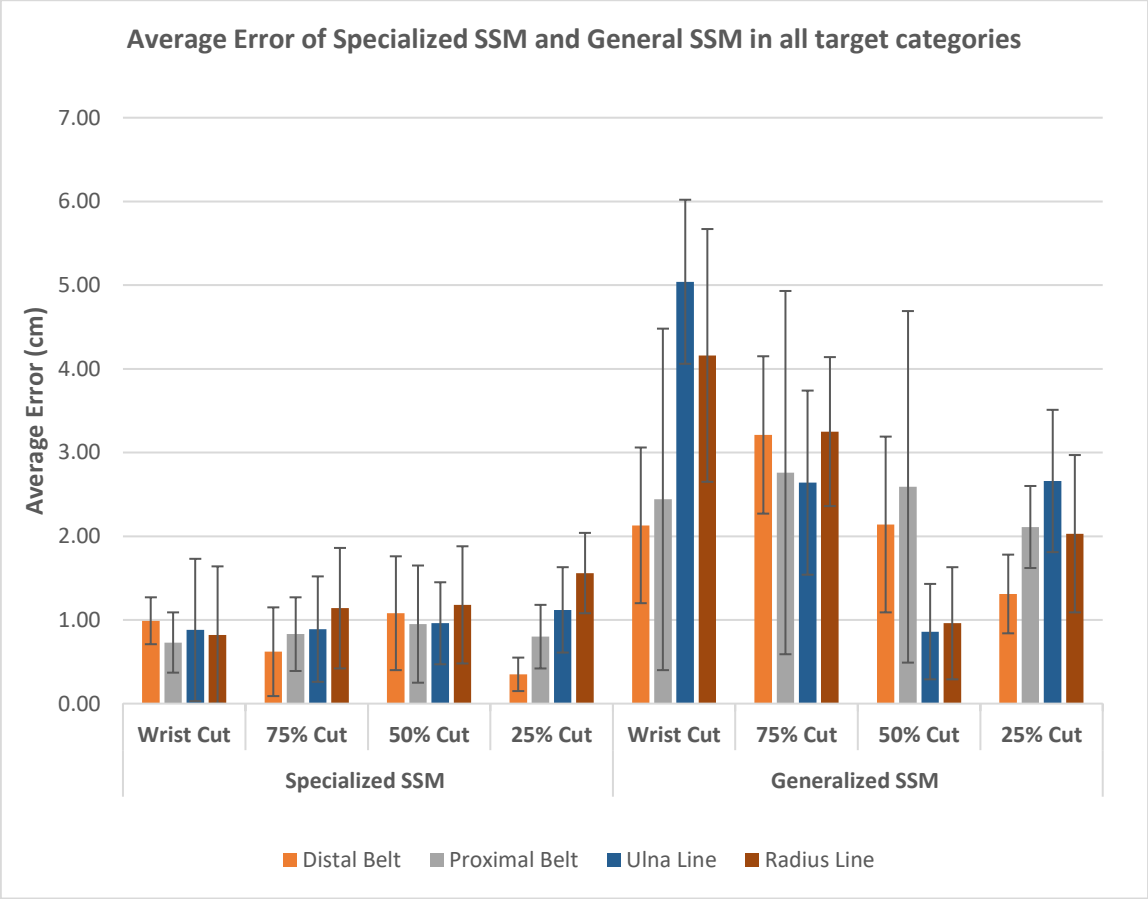

Figure 52. Average Error of Specialized SSM and General SSM in all target categories.

Chapter 5: Discussion

We achieved automatic measurement of the human upper limb digital model.

We have successfully implemented 3D anthropometry methods in order to achieve automatic measurement of the human upper limb digital model. We created a MATLAB code to measure dimensions of a digital upper limb 3D model. The dimensions are used for making a prosthetic socket.

We implemented Statistical Shape Model as the main landmarking algorithm. We used a single SSM and multiple SSM approach to compare which approach performs better in our case. We Implemented Screened Poisson surface reconstruction method and Uniform Remeshing to the training data. We used Rigid and Non-Rigid ICP for the training data surface registration. We used Principal component analysis by using Singular Value Decomposition to build the SSM. The mean surface of the SSM is marked to show important landmark points. New target can be fitted after SSM is finished. We used Active Shape Model followed with local deformation for fitting into a new target. For the measurement method, we used geodesic distance and Intersection Line from regression plane.

The SSM works well to match a new target with low computational cost.

The statistical shape model performs well to match a new surface target with both Specialized SSM and general SSM shows a good result in matching with low computational cost. We assume the input surface is ideal and without error. Time of matching for every SSM in MATLAB using a computer equipped with processor Intel Core i5 2.7 GHz is around 35-40 seconds.

The Specialized SSM showed better performance in measuring the important landmarks.

As shown in Section 4.7 Results, The Specialized SSM has showed a better precision in measuring important dimensions than the General SSM by showing a lower average absolute error and also lower deviation around the absolute error average. The overall average error for Specialized SSM is 0.93 cm with Standard Deviation of 0.48 cm. Whereas the overall average error for General SSM is 2.52 cm with Standard Deviation of 1.62 cm. We can argue that the specialized SSM is more suitable to measure upper limb for prosthetic application.

In Section 4.6.6 Comparison, The Specialized SSM showed that its circumference average error for the Distal Belt and Proximal Belt is 0.76 cm and 0.83, respectively. According to open fitting ring size, the step of each ring is 3 mm diameter, which translates to a 0.942 cm circumference difference. We can assume that our Specialized SSM is sufficient for real life measurement, and since the General SSM circumference error is 2.16 cm and 2.47 cm, it is not acceptable for real life use. In order to prove this, in the future we could have an experiment to automatically measure real upper limb amputee and test the printed prosthetic socket from the measured dimensions.

The Specialized SSM lines average error is significantly lower than General SSM. The Specialized SSM showed error of 0.96 cm and 1.18 cm for Ulna and Radius Line, respectively. Where the General SSM showed error of 2.8 and 2.6 cm for the same instances. This means, by using the Specialized SSM, measurement of lines resulted only 34% and 45% of the general SSM error. In Table 19, the cross

section lines of the specialized SSM are 0.24 cm and 0.47 cm for the width and depth measurement, respectively. These values are better than values produced by the General SSM which give 3.15 cm and 0.75 cm. There is no standard available for the lines acceptable range. However, considering the significant difference, we can argue that the Specialized SSM produced much better result.

Comparison of the automatic measurement with the manual measurement.

We observed observer error from the repeated manual measurement. The average deviation of the circumference measurement is 0.58 cm and the average deviation of the line measurement is 0.44 cm. This is considerably a lower deviation compared to the average error of the SSM measurements and hence it is still a better method than the SSM. However, we believed that the manual measurement is prone to inconsistency due to a possible different angle of the elbow bend between measurements. The automatic measurement is consistent because the 3D model target shape is fixed.

As shown in Table 22 Section 4.7.7, most of Specialized SSMs produced underestimation of measurements, except the measurements for distal belt and proximal belt on the 50% cut. It shows that the SSM of the 50% cut is giving a closer belt location to the elbow. Meanwhile, both overestimation and underestimation of values occured in a similar number of times in Generalized SSM. However the overestimation appeared only on the circumference measurement which is Distal belt and Proximal Belt. All lines measurements are giving an underestimation in both SSM.

We believed that the circumference underestimation of the Specialized SSM is caused by the shrinkage of the target model during the Screened Poisson Surface Recontruction process. Overall, the underestimation result of Specialized SSM itself is not a major issue. However, In the General SSM, the circumference is overestimating by a larger value compared to the Specialized SSM. This happened due to a wrong final location of circumference belt. The Distal Belt is closer to the elbow, producing a big circumference value while the proximal belt are often crossed to the upper arm region. This phenomenon also affect the extreme underestimation of the lines measurement in the General SSM where the distal belt is closer to the proximal belt.

Locations of the surface that show more errors.

In order to determine which location is prone to measurement error, we defined that if the result shows an error more than 1.88 cm (twice the acceptable result), then the location of matching is incorrect. This error appeared most on the Distal Belt. This showed that the Distal Belt vertices are prone to errors.

Furthermore, we observed extreme errors where the values are more than 4 cm. These errors are most apparent on Proximal Belt where the maximum error is 8.14 cm. We found out that the extreme error is result of with wrong location of measurement. For example, the Proximal Belt measurement location has deviated to the upper arm as shown in Figure 53. We tried to compensate this error by putting 2 regression planes on this point, however it does not always solve the problem. Another error is shown in the same figure, as the Distal Belt is morphing too close to the tip of the stump. The Radius and Ulna Lines correlates to The Distal and Proximal Belt. Therefore, when one of them is incorrect, the lower arm lines will also show large error. The wrong measurement of these lines is shown in Figure 54.

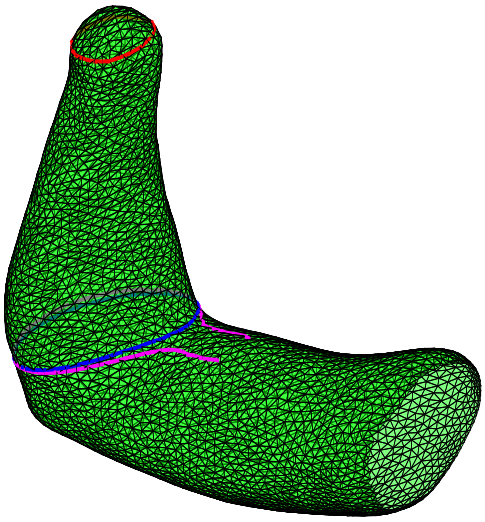

Figure 53. Examples of a wrong measurement. The Distal Belt (Red Line) is too close to tip of the stump. The Proximal Belt (Purple Line) crossed into the upper arm region which resulted in wrong measurement. The second intersection line (Blue Line) is used to compensate if an error happens.

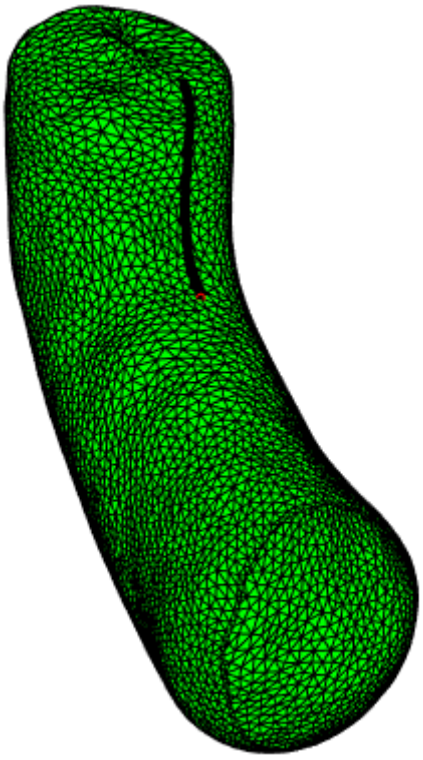

Figure 54. An example of wrong measurement of the Radius Line (Black Line). The algorithm is measuring until upper arm region due to the wrong location of the Proximal Belt.

Rigid alignment is very important in fitting a new target.

In both SSM approach, we observed that initial incorrect rigid alignment fitting could result in a mismatch of belt vertices, which resulted in over-morphing of the vertices. The mismatch might be happening because of the incorrect pose of the subject scan. For example, when the subject is not posing the upper limb in a 90^{o} bending position. The SSM can compensate the bending angle from one of its principal components but not as much. Later, this resulted in a wrong landmarking to the target.

One important aspect when performing a rigid alignment is that the elbow is a crucial location, where it should be the centre of the alignment. Most extreme errors started from wrong a misalignment of the elbow and it resulted in wrong location of elbow points (olecranon and antecubital fossa). An example of initial misalignment shown in Figure 55. The error leads to wrong assignment of important landmark in the target as shown in Figure 56.

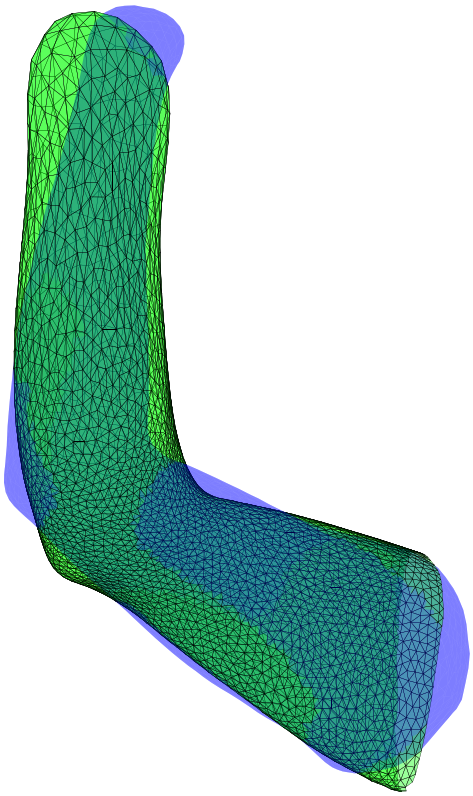

Figure 55. Example of a misalignment error of Rigid Alignment. This resulted in a wrong elbow and tip of the stump locations.

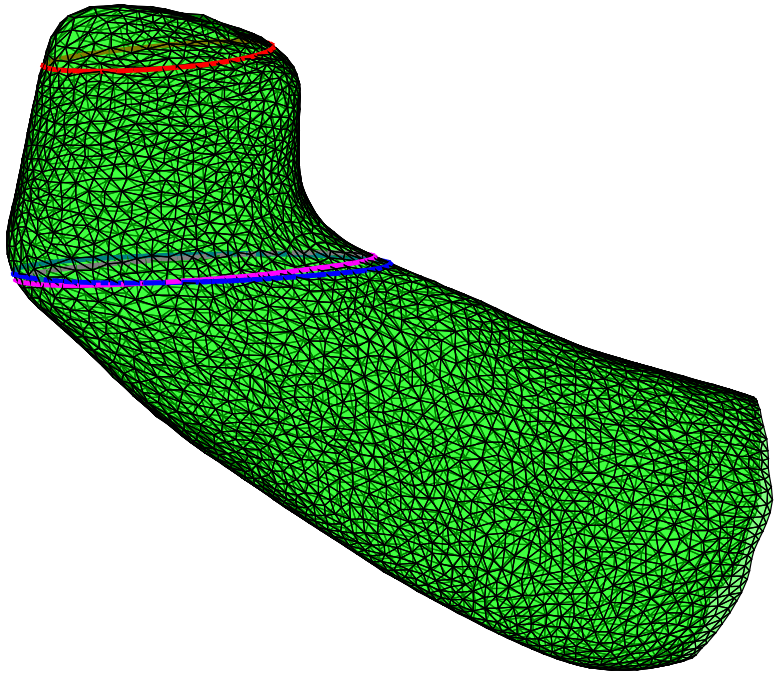

Figure 56. An example of wrong distal (red line) and proximal (purple line) belt result. Due to a failed initial alignment, the SSM vertices match into wrong location on target surface although the surface fitting result is good.

General SSM Remarks

We have discussed about the better results from the specialized SSM in previous statements. However, this result does not mean the performance to match a new target surface of the general SSM is much lower than the specialized SSM. The higher measurement error most likely due to the belt vertices and the landmark points of the general SSM deviates a lot more than the specialized SSM in every category.

This mismatch also could be happening because of the point-to-point Active shape model fitting. Even though we already created targets with the same number vertices with the SSM, the results in fitting new target showed that vertices in stump tip region of the general SSM is widely spaced in the longer arm target as shown in Figure 57 and the vertices are denser on matching the shorter arm targets as shown in Figure 59. Figure 57 and Figure 58 showed that the vertices in the general SSM failed to translate more to achieve further targets from its mean surface. In point-to-plane matching the tubular nature of the lower arm could move further as long it is still on the tangent plane of the target. Therefore, we could try to use point-to-plane matching for future improvement.

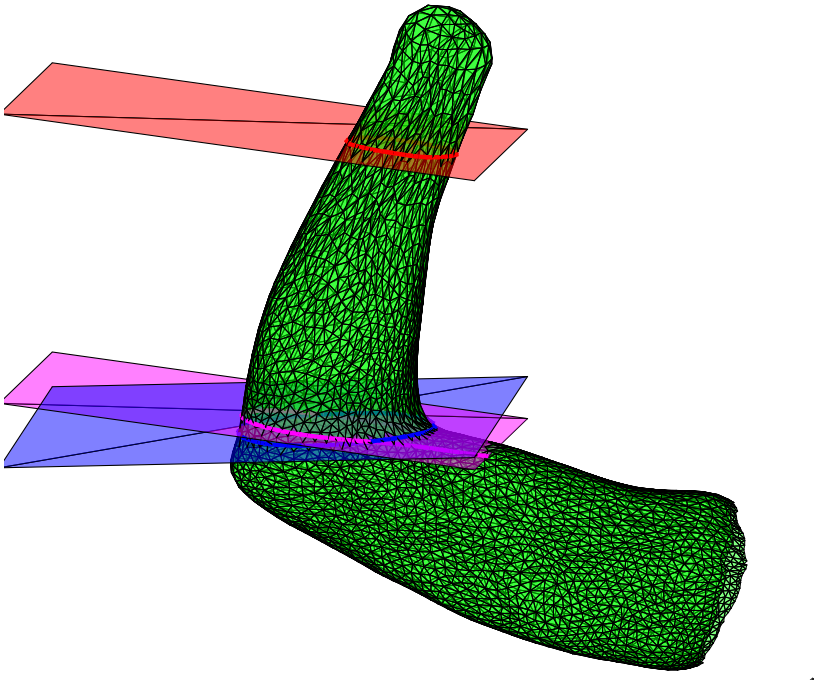

Figure 57. An example of General SSM matching in wrist cut target. The Distal Belt failed to reach the exact location of the wrist even though the surface fitting is good.

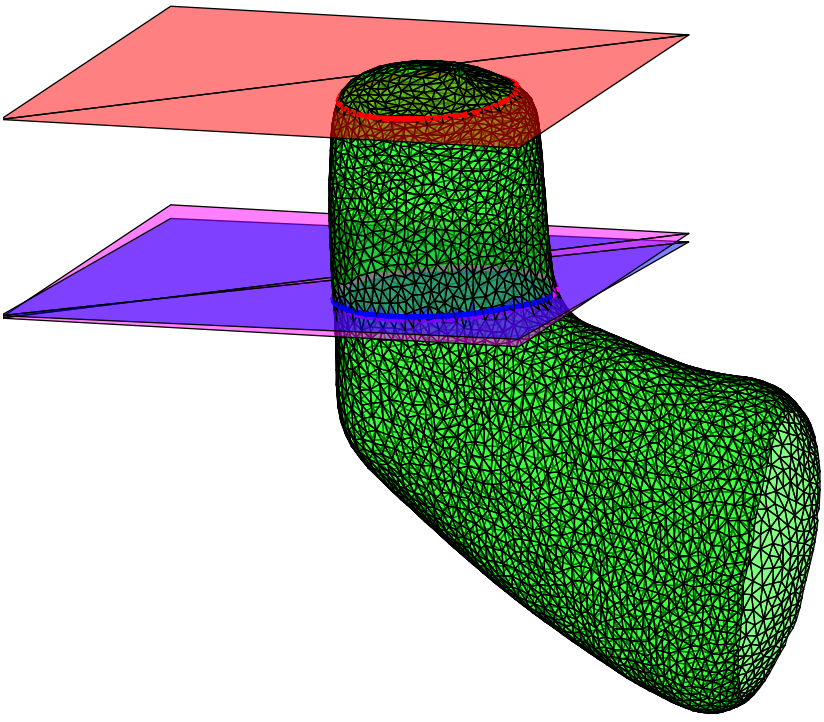

Figure 58. An example of General SSM matching in 25% cut target. The Distal Belt failed to reach further optimal location.

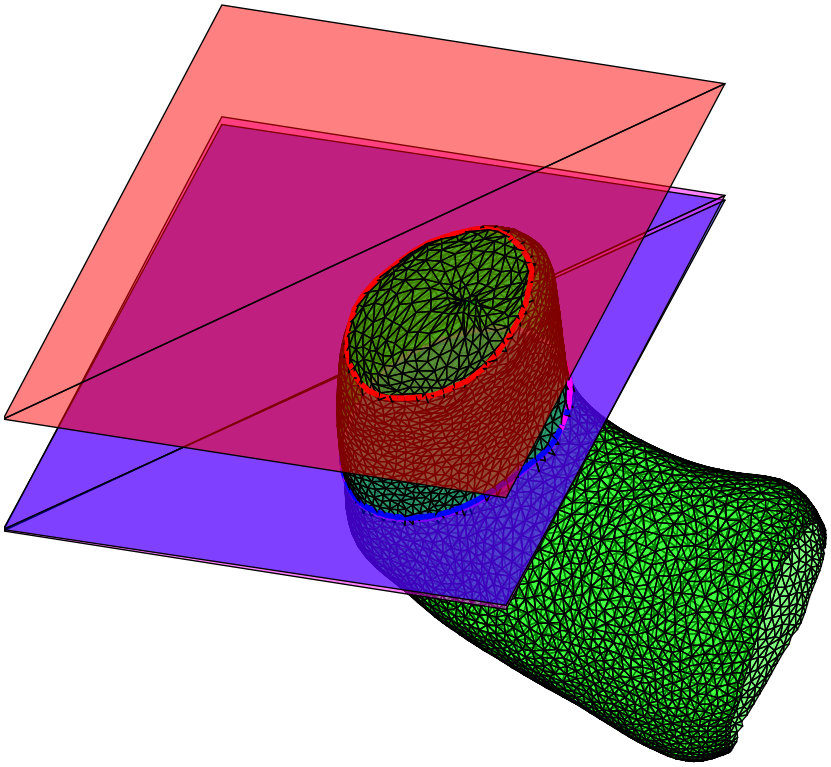

Figure 59. An example of General SSM matching from top view. Vertices near the stump tip region are dense (oversampling).

Future Works

Based on the research findings and problems that we encountered, we would like to recommend a few points to improve the research on automatic measurement of upper limb for prosthetic application:

- Improvement of the general SSM by vertex-to-plane surface registration. The General SSM showed a failure in translating the vertices to the optimal location in the further targets. We believed this happened due to the vertex-to-vertex fitting algorithm only translate the vertices in the tip of stump without maintaining the balance of vertices sampling. Another approach is to have a different algorithm which always provide exact Distal Belt offset from the tip of stump.
- Using a better Rigid Alignment by marking of elbow points if possible. The marked points can be aligned with the SSM surface with better result and avoid bad initial misalignment.
- Provide guideline for a scanning procedure to avoid wrong upper limb pose in 3D model acquisition. We saw some wrong measurement due to initial misalignment. This happened because the 3D model upper limb is not posing in 90^{o} angle. 3D models which posed close to 90^{o} angle are less affected from this problem.
- Improve the experiment by producing the 3D printed socket with a real amputee measurement and assess the produced socket fit quality. We can ensure the fit quality of the measurement and improve the algorithm based on the result found from the improved experiment.

Chapter 6: Conclusion of the Thesis

We achieved automatic measurement of the human upper limb digital model for prosthetic application. Our automatic measurement algorithm proved that we can measure a real human upper limb without human intervention. The research showed that the multiple statistical shape model is a better approach for measuring lower arm amputation. The multiple SSM approach or what we call 'Specialized SSM' showed a robust performance over a big variation of the residual arm length.

We managed to answer the research question by creating a Statistical Shape Model and an algorithm which incorporated Active Shape Model, Geodesic Distances and Intersection Line to automatically measure the upper limb dimensions. The required measurement for creating a socket are Ulna and Radius Lines, and lower arm proximal and distal circumferences. The algorithm will produce these dimensions for design parameter of the 3D printed prosthetic socket. The average circumference error from the Specialized SSM algorithm are 0.76 cm and 0.86 cm for the Distal and Proximal circumference, which is a sufficient result. Therefore, it can be used for real prosthetic application assuming the input 3D surface is ideal.

From the experiment, we can reflect that our automatic 3D measurement is not perfect yet. There are many errors that could happen from different aspects. Potential improvement of the algorithm are implementation of a better rigid alignment and method change of the SSM fitting by using point-to-plane surface registration. With the current result, it is possible to implement this algorithm in the 3D printed upper limb prosthesis project. In the future, we suggest inviting upper limb amputees as the experiment subject and produce the resulting socket to see how well the automatic measurement works on real life.

The future of prosthetic device accessibility can be leveraged with smartphone and 3D printing. This '3D printed prosthetic hand by using a smartphone' project is another step that showed technology development could help everyone afford the access to assistance for their needs.

References

[1] S. B. Cooke and C. E. Terhune, “Form, function, and geometric morphometrics.,” *Anat. Rec. (Hoboken).*, vol. 298, no. 1, pp. 5–28, Jan. 2015.

[2] “Colombian Military Hospital Expands Prosthesis Program.” [Online]. Available: https://dialogo-americas.com/en/articles/colombian-military-hospital-expands-prosthesis-program. [Accessed: 22-Sep-2018].

[3] “How 3D printed prosthetic limbs are helping one hospital treat Syrian war refugees.” [Online]. Available: https://newatlas.com/3d-printed-prostheses-syria/53685/. [Accessed: 09-Oct-2018].

[4] T. C. B. Grant McGimpsey, “Limb Prosthetics Services and Devices Critical Unmet Need: Market Analysis,” 2008.

[5] Ł. Markiewicz, M. Witkowski, R. Sitnik, and E. Mielicka, “3D anthropometric algorithms for the estimation of measurements required for specialized garment design,” *Expert Syst. Appl.*, vol. 85, pp. 366–385, 2017.

[6] R. Suikerbuik, H. Tangelder, H. Daanen, and A. Oudenhuijzen, “Automatic feature detection in 3D human body scans,” *SAE Tech. Pap.*, 2004.

[7] J. Niu, Y. Zhang, and J. Wu, “Challenges in the application of three-dimensional anthropometry,” in *2009 4th IEEE Conference on Industrial Electronics and Applications, ICIEA 2009*, 2009, pp. 864–868.

[8] B. Azouz, Z. Ben, and A. Chang, “Automatic Locating of Anthropometric Landmarks on 3D Human Models * Automatic Locating of Anthropometric Landmarks on 3D Human Models,” no. 3dpvt, 2006.

[9] C. Lovato, U. Castellani, S. Fantoni, C. Milanese, C. Zancanaro, and A. Giachetti, *Computer assisted estimation of anthropometric parameters from whole body scanner data*, vol. 5903 LNCS. 2009.

[10] I. F. Leong, J. J. Fang, and M. J. Tsai, “Automatic body feature extraction from a marker-less scanned human body,” *CAD Comput. Aided Des.*, vol. 39, no. 7, pp. 568–582, 2007.

[11] J.-M. Lu and M.-J. J. Wang, “Automated anthropometric data collection using 3D whole body scanners,” *Expert Syst. Appl.*, vol. 35, no. 1–2, pp. 407–414, 2008.

[12] W. Lee, S. Yoon, and H. You, “Development of a 3D semi-automatic measurement protocol for hand anthropometric measurement,” in *Proceedings of the Human Factors and Ergonomics Society*, 2010, vol. 3, pp. 1780–1784.

[13] H. Boukamcha, M. Elhallek, M. Atri, and F. Smach, “3D face landmark auto detection,” in *2015 World Symposium on Computer Networks and Information Security, WSCNIS 2015*, 2015.

[14] S. Gupta, M. K. Markey, and A. C. Bovik, “Anthropometric 3D face recognition,” *Int. J. Comput. Vis.*, vol. 90, no. 3, pp. 331–349, 2010.

[15] H. Han and Y. Nam, “Automatic body landmark identification for various body figures,” *Int. J. Ind. Ergon.*, vol. 41, no. 6, pp. 592–606, 2011.

[16] J. C. Liu, L. Zhang, X. Chen, and J. W. Niu, “Facial landmark automatic identification from three dimensional (3D) data by using Hidden Markov Model (HMM),” *Int. J. Ind. Ergon.*, vol. 57, pp. 10–22, 2017.

[17] “ISO 20685 web page.” [Online]. Available: https://www.iso.org/standard/63261.html.

[18] L. Seoud, J. Ramsay, S. Parent, and F. Cheriet, “A novel fully automatic measurement of apparent breast volume from trunk surface mesh.,” *Med. Eng. Phys.*, vol. 41, pp. 46–54, Mar. 2017.

[19] Y. Ding *et al.*, “An automatic method of measuring foot girths for custom footwear using local RBF implicit surfaces,” *Int. J. Comput. Integr. Manuf.*, vol. 23, no. 6, pp. 574–583, 2010.

[20] F. L. Bookstein, “Morphometric Tool for Landmark Data,” *Biometrics*, vol. 54, no. 1, p. 398.

[21] G. W. Weber, F. L. Bookstein, and D. S. Strait, “Virtual anthropology meets biomechanics.,” *J. Biomech.*, vol. 44 8, pp. 1429–1432, 2011.

[22] “ISO 7250-1:2017,” 2017. [Online]. Available: https://www.iso.org/standard/65246.html. [Accessed: 13-May-2018].

[23] Y. li and Y. Zhong, “Automatic detecting anthropometric landmarks based on spin image,” *Text. Res. J.*, vol. 82, no. 6, pp. 622–632, 2012.

[24] M.-J. J. Wang, W.-Y. Wu, K.-C. Lin, S.-N. Yang, and J.-M. Lu, “Automated anthropometric data collection from three-dimensional digital human models,” *Int. J. Adv. Manuf. Technol.*, vol. 32, no. 1–2, pp. 109–115, 2007.

[25] S. Y. Fang and J. J. Fang, “Automatic head and facial feature extraction based on geometry variations,” *CAD Comput. Aided Des.*, vol. 43, no. 12, pp. 1729–1739, 2011.

[26] J. Guo, X. Mei, and K. Tang, “Automatic landmark annotation and dense correspondence registration for 3D human facial images,” *BMC Bioinformatics*, vol. 14, no. 1, 2013.

[27] S. Sghaier, C. Souani, H. Faeidh, and K. Besbes, “Novel Technique for 3D Face Segmentation and Landmarking,” *2016 Glob. Summit Comput. Inf. Technol.*, pp. 27–31, 2016.

[28] C. Lovato, U. Castellani, and A. Giachetti, “Automatic Segmentation of Scanned Human Body Using Curve Skeleton Analysis,” *Lect. Notes Comput. Sci.*, 2009.

[29] A. Giachetti, C. Lovato, F. Piscitelli, C. Milanese, and C. Zancanaro, “Robust automatic measurement of 3D scanned models for the human body fat estimation.,” *IEEE J. Biomed. Heal. informatics*, vol. 19, no. 2, pp. 660–667, Mar. 2015.

[30] J. C. Liu, L. Zhang, X. Chen, and J. W. Niu, “Facial landmark automatic identification from three dimensional (3D) data by using Hidden Markov Model (HMM),” *Int. J. Ind. Ergon.*, vol. 57, pp. 10–22, 2017.

[31] K. V. Mardia and I. L. Dreden, *Statistical Shape Analysis : with application in R*. New York: John Wiley, 1998.

[32] H. Abbas, Y. Hicks, and D. Marshall, “Automatic classification of facial morphology for medical applications,” in *Procedia Computer Science*, 2015, vol. 60, no. 1, pp. 1649–1658.

[33] A. Kermi and M. T. Laskri, “A 3D deformable model constrained by anthropometric knowledge for computerized facial reconstructions,” in *2012 11th International Conference on Information Science, Signal Processing and their Applications, ISSPA 2012*, 2012, pp. 924–929.

[34] Z. Zhou and S. Hao, “Anatomical landmark detection on 3D human shapes by hierarchically utilizing multiple shape features,” *Neurocomputing*, vol. 253, pp. 162–168, 2017.

[35] X. Zhang, N. Fan, X. Chen, L. H. Ran, and J. W. Niu, “Feature extraction of three dimensional (3D) facial landmarks using spin image,” in *IEEM2010 - IEEE International Conference on Industrial Engineering and Engineering Management*, 2010, pp. 537–541.

[36] F. M. Sukno, J. L. Waddington, and P. F. Whelan, “3-D Facial Landmark Localization with Asymmetry Patterns and Shape Regression from Incomplete Local Features,” *IEEE Trans. Cybern.*, vol. 45, no. 9, pp. 1717–1730, 2015.

[37] G. Böer, F. Hahmann, H. Essig, and F. Kiel, “Detection of Facial Landmarks in 3D Face Scans Using the Discriminative Generalized Hough Transform (DGHT),” no. March, 2017.

[38] C. Lovato, U. Castellani, C. Zancanaro, and A. Giachetti, “Automatic labelling of anatomical landmarks on 3D body scans,” *Graph. Models*, vol. 76, no. 6, pp. 648–657, 2014.

[39] C. Loconsole, N. Barbosa, A. Frisoli, and V. Costa Orvalho, *A new marker-less 3D kinect-based system for facial anthropometric measurements*, vol. 7378 LNCS. 2012.

[40] S. Jahanbin, H. Choi, and A. C. Bovik, “Passive multimodal 2-D+3-D face recognition using gabor features and landmark distances,” *IEEE Trans. Inf. Forensics Secur.*, vol. 6, no. 4, pp. 1287–1304, 2011.

[41] A. J. Naftel and M. J. Trenouth, “Stereo-assisted landmark detection for the analysis of changes in 3-D facial shape,” *Informatics Heal. Soc. Care*, vol. 29, no. 2, pp. 137–155, 2004.

[42] B. Azouz, Z. Ben, and A. Chang, “Automatic Locating of Anthropometric Landmarks on 3D Human Models,” no. 3dpvt, 2006.

[43] Y. Zhang and S. Xu, “Data-driven feature-based 3D face synthesis,” in *3DIM 2007 - Proceedings 6th International Conference on 3-D Digital Imaging and Modeling*, 2007, pp. 39–46.

[44] T. Cootes, “An Introduction to Active Shape Models,” *Image Process. Anal.*, 2000.

[45] B. Amberg, S. Romdhani, and T. Vetter, “Optimal Step Nonrigid ICP Algorithms for Surface Registration,” in *2007 IEEE Conference on Computer Vision and Pattern Recognition*, 2007, pp. 1–8.

[46] H. Li, R. W. Sumner, and M. Pauly, “Global Correspondence Optimization for Non-Rigid Registration of Depth

Scans," *Comput. Graph. Forum*, vol. 27, no. 5, pp. 1421–1430.

[47] S. Liang, J. Wu, S. M. Weinberg, and L. G. Shapiro, "Improved detection of landmarks on 3D human face data," *Conf. Proc. ... Annu. Int. Conf. IEEE Eng. Med. Biol. Soc. IEEE Eng. Med. Biol. Soc. Annu. Conf.*, vol. 2013, pp. 6482–6485, 2013.

[48] G. Böer, F. Hahmann, H. Essig, and F. Kiel, "Detection of Facial Landmarks in 3D Face Scans Using the Discriminative Generalized Hough Transform (DGHT)," no. March, 2017.

[49] H. Han, Y. Nam, and S. Hwang Shin, "Algorithms of the Automatic Landmark Identification for various torso shapes," *Int. J. Cloth. Sci. Technol.*, vol. 22, no. 5, pp. 343–357, 2010.

[50] M. Kouchi and M. Mochimaru, "Errors in landmarking and the evaluation of the accuracy of traditional and 3D anthropometry," *Appl. Ergon.*, vol. 42, no. 3, pp. 518–527, 2011.

[51] J. Li, M. Sun, H.-C. Chen, Z. Li, and W. Jia, "Anthropometric measurements from multi-view images," in *2012 38th Annual Northeast Bioengineering Conference, NEBEC 2012*, 2012, pp. 426–427.

[52] O. Wasenmüller, J. C Peters, V. Golyanik, and D. Stricker, "Precise and Automatic Anthropometric Measurement Extraction Using Template Registration." 2015.

[53] M. Pogosian and D. H. Plettenburg, "Design of 2nd generation WILMER Open Socket," Delft University of Technology, 2015.

[54] D. H. Plettenburg, *Upper extremity prosthetics: Current status & evaluation*. Delft University of Technology, 2002.

[55] W. Walta, S. Naumann, and M. Milner, "Ergonomic socket design for congenital below elbow amputated children," *J. Rehabil. Med.*, vol. 2, pp. 19–24, 1989.

[56] J. Yat and L. Wong, "Redesign of a fitting for an upper extremity prosthesis," Delft University of Technology, 2008.

[57] M. Moreo, "Parametric design of a 3D printable hand prosthesis for children in developing countries," 2016.

[58] M. Kazhdan and H. Hoppe, "Screened Poisson Surface Reconstruction," *ACM Trans. Graph.*, vol. 32, no. 3, p. 29:1--29:13, Jul. 2013.

[59] S. Valette, J.-M. Chassery, and R. Prost, "Generic Remeshing of 3D Triangular Meshes with Metric-Dependent Discrete Voronoi Diagrams," *IEEE Trans. Vis. Comput. Graph.*, vol. 14, pp. 369–381, 2008.

[60] D. S. Richardson, "Euler's Gem: The Polyhedron Formula and the Birth of Topology," *Math. Intell.*, p. 336, 2008.

[61] C. Goodall, "Procrustes Methods in the Statistical Analysis of Shape," *J. R. Stat. Soc. Ser. B*, vol. 53, no. 2, pp. 285–339, 1991.

[62] J. Mitchell, D. Mount, and C. Papadimitriou, "The Discrete Geodesic Problem," *SIAM J. Comput.*, vol. 16, no. 4, pp. 647–668, 1987.